Atomic layer deposition of thin films: from a chemistry perspective

OPEN ACCESS
IOP Publishing | IMMT
International Journal of Extreme Manufacturing
Int. J. Extrem. Manuf. **5** (2023) 032003 (29pp)
https://doi.org/10.1088/2631-7990/acd88e

Topical Review

Atomic layer deposition of thin films: from a chemistry perspective

Jinxiong Li[1], **Gaoda Chai**[2] **and Xinwei Wang**[1,*]

[1] School of Advanced Materials, Shenzhen Graduate School, Peking University, Shenzhen 518055, People's Republic of China
[2] Huawei Technologies Co., Ltd, Shenzhen 518129, People's Republic of China

E-mail: wangxw@pkusz.edu.cn

Received 16 November 2022, revised 12 February 2023
Accepted for publication 24 May 2023
Published 14 June 2023

Abstract

Atomic layer deposition (ALD) has become an indispensable thin-film technology in the contemporary microelectronics industry. The unique self-limited layer-by-layer growth feature of ALD has outstood this technology to deposit highly uniform conformal pinhole-free thin films with angstrom-level thickness control, particularly on 3D topologies. Over the years, the ALD technology has enabled not only the successful downscaling of the microelectronic devices but also numerous novel 3D device structures. As ALD is essentially a variant of chemical vapor deposition, a comprehensive understanding of the involved chemistry is of crucial importance to further develop and utilize this technology. To this end, we, in this review, focus on the surface chemistry and precursor chemistry aspects of ALD. We first review the surface chemistry of the gas–solid ALD reactions and elaborately discuss the associated mechanisms for the film growth; then, we review the ALD precursor chemistry by comparatively discussing the precursors that have been commonly used in the ALD processes; and finally, we selectively present a few newly-emerged applications of ALD in microelectronics, followed by our perspective on the future of the ALD technology.

Keywords: atomic layer deposition, surface reaction, precursor, chemical mechanism

1. Introduction

Following the Moore's law, the critical size of the microelectronic devices has been continually shrinking over the decades to boost the performance of the integrated circuits (ICs) [1]. As the device critical size gradually approaches its limit, more efforts have been made to explore new materials and 3D device structures to further extend the Moore's law. Owing to the limitation by short-channel effects, non-planer field-effect transistors (FETs), such as fin FETs (FinFETs) [2] and gate-all-around (GAA) FETs [3], have been gradually adopted in the microelectronics industry. To meet the requirements of fabricating chips with these complex structures, it is very important to use a deposition technology that can controllably afford highly uniform conformal thin films on 3D topologies. Atomic layer deposition (ALD) is an essential technology for these purposes. ALD is based on sequential and self-limiting gas–solid chemical reactions, and owing to the self-limiting nature, the composition and thickness of the deposited thin films can be precisely controlled at the atomic scale [4–6]. Also, ALD is able to deposit highly uniform films in trench or hole structures with a high aspect ratio, which can hardly be achieved by the conventional physical vapor deposition

* Author to whom any correspondence should be addressed.

(PVD) or chemical vapor deposition (CVD). Over the past decades, along with the downscaling of the microelectronic devices, ALD has become extensively used in numerous key process steps in the advanced technology nodes of the IC fabrication, such as the deposition of ultrathin high-k oxides for the gate-dielectrics in FETs [7, 8] and the capacitor-dielectrics in dynamic random access memory (DRAM) [9, 10], the deposition of the spacers for self-aligned multi-patterning [11, 12], etc. Also, ALD is essential for the preparation of many newly-emerged microelectronic devices, such as the back-end-of-line (BEOL)-compatible oxide-based transistors [13–15]. Therefore, the ALD technology has been considered as a vital enabler to realize new device structures for ICs.

The ALD technology relies heavily on the involved surface chemistry, which can significantly influence the properties of the deposited films, such as film thickness, morphology, conformality, and composition. Therefore, a comprehensive understanding of the surface chemistry and associated mechanisms is very important. The ALD precursors are also very important; they are usually metalorganic compounds, and their volatility, thermal stability, and self-limiting reactivity can substantially affect the growth behavior of the ALD films. Therefore, the design of the precursor chemical structures is of the pivot for the ALD technology.

To address the above issues, this review focuses on the chemistry aspect of the ALD technology. The chemistry involved in the ALD surface reactions is firstly reviewed, and the associated mechanisms are elaborately discussed. Then follows the review of the precursor chemistry, and the precursors that have been commonly used are carefully discussed. Finally, the applications of the ALD technology for some newly-emerged areas in microelectronics are discussed. Certainly, we cannot review every aspect of the ALD technology, given its already very wide applications, and the readers may refer to some other published reviews for more information about ALD [16–30].

2. Surface chemistry of ALD

ALD is essentially a variant of CVD. An ALD process relies on two or more self-limiting gas–solid chemical reactions, which are controlled to proceed in an alternate and cyclic manner. As shown in figure 1(a), a typical ALD process consists of a cycling of four steps: (I) excessive amount of precursor A is dosed into the chamber to react with the functional groups on the solid surface, and the reaction is self-limiting and the byproduct is volatile; (II) the chamber is purged by inert gas to completely remove the byproduct and unreacted A; (III) excessive amount of precursor B is dosed into the chamber to react with the functional groups formed in (I), and the reaction is also self-limiting and the byproduct is also volatile; and (IV) the chamber is again purged by inert gas to completely remove the byproduct and unreacted B.

The key point of ALD is that the gas–solid chemical reactions should be self-limiting, and this feature is illustrated in figure 1(b), where the gas–solid chemical reactions can be regarded as the chemisorption of the precursor on the solid surface and the chemisorption saturates as the precursor exposure amount exceeds a certain point. The saturated chemisorption can afford a fixed amount of material grown on the surface in each ALD cycle. Therefore, a uniform thin film of material can be conformally coated on any structured surfaces, and at the same time, the film thickness can be precisely controlled by the number of the ALD cycles. On the other hand, insufficient precursor exposure would lead to unsaturated chemisorption on the surface, and the remaining active surface sites are still capable of adsorbing a second type of precursor. This strategy has been used in the ALD of multi-element compounds. For instance, a ternary oxide $A_xB_yO_z$ can be deposited by the pulsing sequence of the A, B, and O precursors, where the pulse of A is set in the subsaturation regime [31, 32].

The surface chemical reactions are normally temperature dependent (figure 1(c)), and the temperature range where the surface reactions are self-limiting is regarded as the ALD window. Although the film growth rate (also known as growth per cycle, GPC) is often a constant within the window, the range of the ALD window is actually bounded by the fulfillment of the self-limiting conditions; and therefore, GPC in the window may increase or decrease as well. Precursor condensation or incomplete reaction may occur below the window; whereas precursor decomposition or desorption may occur above the window.

As the surface chemical reactions are crucial for ALD, a thorough understanding of the associated mechanisms is very important to develop and optimize the ALD processes in order to achieve the desired film properties, such as the film thickness, morphology, conformality, and composition. Among the ALD processes that have been so far realized for numerous materials, the involved ALD surface chemistry mechanisms can be generally classified into four categories, which are the ligand-exchange, dissociative or non-dissociative chemisorption, oxidation, and reduction mechanisms. The attributes of these mechanisms are elaborated as follows.

2.1. Ligand-exchange mechanism

The ligand-exchange mechanism (figure 2(a)) is the most common mechanism for ALD, and it can be described as the following general reaction scheme:

$$||-a + ML_n(g) \;\rightarrow\; ||-ML_{n-1} + aL(g), \qquad (1)$$

where || denotes the surface, a is a surface group, M is a metal atom, and L is a ligand of the precursor. During the ligand-exchange reaction, a ligand (L) of the gaseous precursor molecule (ML_n) is displaced by the surface species ($||-a$), forming the volatile byproduct of aL, and meanwhile, the remainder of the precursor molecule bonds to the surface, forming a chemisorbed new surface species of $||-ML_{n-1}$. The ligand-exchange reaction may continue to occur between the chemisorbed $||-ML_{n-1}$ and another nearby $||$-a surface

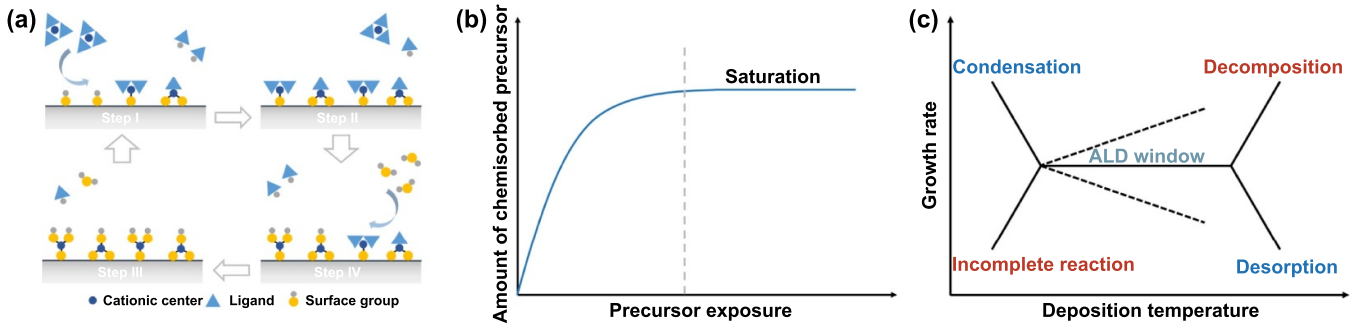

Figure 1. Characteristics of ALD. (a) Schematic illustration of an ALD cycle. (b) Saturation behavior of the precursor chemisorption. (c) Temperature dependence of the ALD film growth rate.

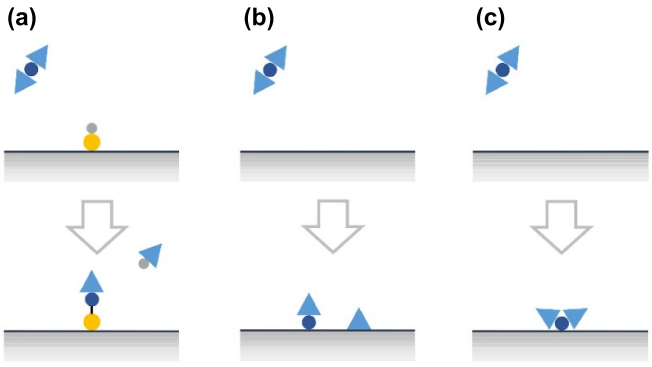

Figure 2. Schematic illustration of the chemisorption mechanisms: (a) ligand-exchange, (b) dissociative chemisorption, and (c) non-dissociative chemisorption mechanisms.

group, and therefore, multiple chemical bonds may be formed between the precursor and surface as the following:

$$||-ML_{n-1} + \; ||-a \rightarrow ||-ML_{n-2}-|| \; + aL(g)\,. \qquad (2)$$

A common example of the ligand-exchange mechanism is the proton transfer scheme, in which a Brønsted base abstracts a proton from a Brønsted acid. As the scheme shown in equation (1), the metal precursor (ML_n) serves as a Brønsted base, and it can abstract protons (a = H) from the Brønsted acidic surface groups, such as hydroxyls. In this respect, the metal precursor with a stronger ionic character of its metal–ligand bond is more favorable for the proton transfer reaction, because in this case the ligand is more analogous to a free anion and hence more effective to abstract a positively charged proton. The acidity of the ligand itself is also very important; a stronger basic ligand is more effective to abstract a proton, and this effect is well manifested when comparing the precursors of metalorganics and metal halides.

The ALD of Al_2O_3 from the precursors of trimethylaluminum (TMA) and H_2O is a typical process that follows the proton-transfer ligand-exchange mechanism. This ALD process has been extensively studied both experimentally and theoretically [33–35]. In the TMA half-cycle, the surface terminal –OH groups react with the TMA via the proton-transfer ligand-exchange reaction, forming the O–Al bonds and releasing the volatile byproduct of CH_4, and then, in the subsequent H_2O half-cycle, the remaining surface methyl ligands are displayed by hydroxyls via another proton-transfer ligand-exchange reaction with the incoming H_2O molecules:

$$\|-\mathrm{OH} + \mathrm{Al(CH_3)_3\,(g)} \rightarrow \| - \mathrm{O} - \mathrm{Al(CH_3)_2} + \mathrm{CH_4\,(g)}\,, \qquad (3)$$

$$\|-\mathrm{Al} - \mathrm{CH_3} + \; \mathrm{H_2O\,(g)} \rightarrow \| - \mathrm{Al} - \mathrm{OH} \; + \; \mathrm{CH_4\,(g)}\,. \qquad (4)$$

The formation of the strong Al–O bonds is the main driving force for the surface reactions, and the reaction enthalpy was reported to be one of the highest among all ALD reactions [4]. Both the above reactions are efficient and self-limiting, which makes the ALD of Al_2O_3 an almost ideal case for ALD.

The halogen transfer is another example of the ligand-exchange mechanism. The halogen transfer appears in the thermal ALD of W and Mo metals [36, 37], where Si_2H_6 is typically used with the metal fluorides of WF_6 and MoF_6. In these ALD processes, the silane can abstract the fluorine atoms from the surface, forming volatile fluorosilanes, such as SiF_4 and $SiHF_3$, along with H_2 and HF. For instance, the chemical reaction for the ALD of W from WF_6 and Si_2H_6 were found to be [38]

$$\|-\mathrm{W} - \mathrm{SiHF_2}^* \; + \; \mathrm{WF_6\,(g)} \rightarrow \| - \mathrm{W} - \mathrm{WF_5}^* \; + \; \mathrm{SiHF_3\,(g)}\,, \qquad (5)$$

$$\|-\mathrm{W} - \mathrm{WF_5}^* \; + \; \mathrm{Si_2H_6\,(g)} \rightarrow \| - \mathrm{WW} - \mathrm{SiHF_2}^* \; + \; \mathrm{SiHF_3\,(g)} \; + \; \mathrm{2H_2\,(g)}\,. \qquad (6)$$

These reactions are highly exothermic, owing to the formation of the strong Si–F bonds. Simultaneously, the H_2 gas is produced by the reductive elimination of the hydrogen atoms of the unstable intermediate metal hydrides, which are formed by the fluorine-transfer ligand-exchange reaction. The reductive elimination also affords the desired metal films, and further details of the reduction mechanism will be discussed in section 2.4.

Another type of the ligand-exchange mechanism is based on the exchange of the ligands between two metal precursors, which appears in the ALD of Cu and Co metals [39, 40]. As an example, Cu metal can be deposited from bis(dimethylamino-2-propoxy)copper(II) [$Cu(dmap)_2$] and diethylzinc (DEZ). In this ALD process, the surface dmap groups from $Cu(dmap)_2$ are displaced by the ethyls from DEZ via the ligand exchange reaction, forming volatile $Zn(dmap)_2$. The afforded $–Cu(C_2H_5)$ surface species are not stable and readily forms Cu metal and butane through the reductive elimination as the following:

$$2\,\|{-}\mathrm{Cu}-\mathrm{dmap}\ +\ \mathrm{Zn(C_2H_5)_2\,(g)} \rightarrow 2\|-\mathrm{Cu}-\ \mathrm{(C_2H_5)} + \mathrm{Zn(dmap)_2\,(g)}, \tag{7}$$

$$2\,\|{-}\mathrm{Cu}-\ \mathrm{(C_2H_5)} \rightarrow 2\|-\mathrm{Cu^0} + \mathrm{C_4H_{10}\,(g)}. \tag{8}$$

Notably, for all these ligand-exchange mechanisms, it is important that one of the exchanged products is sufficiently volatile to be liberated from the surface, as otherwise, nonideal issues would occur, as will be discussed later. Generally, the ligand-exchange mechanisms are essential for the majority of the ALD processes.

2.2. Dissociative or non-dissociative chemisorption

The chemisorption of the precursors can also follow a dissociative or non-dissociative mechanism. In the dissociative chemisorption scheme (figure 2(b)), the precursor molecule dissociates into two or more parts when it is chemisorbed on the surface,

$$\|\ +ML_n \rightarrow\ \|\,{-}ML_{n-1}{+}\|\ -L. \tag{9}$$

This mechanism often occurs on the surfaces with catalytic activity. For instance, noble metals, such as Ru, have good catalytic nature, and therefore, the ALD processes to deposit Ru often involve the dissociative chemisorption of the ruthenium precursors [41, 42]. Similar processes were also observed on Ni [43, 44] and Cu [45] surfaces. The dissociative chemisorption can also occur on the SiO_2 surface, where strained siloxane (Si–O–Si) bridges are present. For instance, $Al(CH_3)_3$ can be dissociatively chemisorbed on SiO_2 via the following reaction:

$$\|{-}\mathrm{Si-O-Si}{-}\|\ +\ \mathrm{Al(CH_3)_3} \rightarrow \|{-}\mathrm{Si-CH_3} + \|\ -\mathrm{Si-O-Al(CH_3)_2}. \tag{10}$$

In comparison, in the non-dissociative chemisorption mechanism (figure 2(c)), the precursor molecule is adsorbed as a whole on the surface:

$$\|{-}a + ML_n \rightarrow \|-a-ML_n. \tag{11}$$

This mechanism usually occurs when the precursor and surface functional group can form a Lewis acid–base complex. It should be noted that the non-dissociative chemisorption is different from the physisorption, where only weak intermolecular force is present. Nevertheless, the physisorption is often required for a molecule to enter into the chemisorption potential well, especially for the cases without prior activation (e.g. plasma). In the non-dissociative chemisorption, a strong dative bond is formed, and it also has the surface saturation feature. For instance, $Al(CH_3)_3$ has an empty Al 3p orbital, which is capable of accepting additional electrons, and therefore, it can associatively chemisorb on the surface hydroxyl or siloxane bridge, forming a dative bond between the Al and O atoms [46, 47]:

$$\big\|{-}\mathrm{OH}\ +\ \mathrm{Al(CH_3)_3} \rightarrow \big\|-\mathrm{OH-Al(CH_3)_3}, \tag{12}$$

$$\|{-}\mathrm{Si-O-Si}{-}\|\ +\ \mathrm{Al(CH_3)_3} \rightarrow \big\|{-}\mathrm{Si-OAl(CH_3)_3-Si}{-}\big\|. \tag{13}$$

The experimental identification of the species in the non-dissociative chemisorption is challenging, and most of the previous research focused on the theoretical calculations. Nevertheless, the non-dissociative chemisorption is often considered as the first step of the ALD surface reactions, and thus, it may have a profound effect to influence the subsequent reaction pathways.

2.3. Oxidation mechanism

The oxidation mechanism is closely related to the combustion reactions, which appear in many ALD processes to deposit metal oxides and noble metals. In this respect, strong oxidants, such as O_2, O_3, and O_2 plasma, are often used to combust the surface ligands, which normally produces CO_2 and H_2O as the byproducts [48, 49],

$$\|{-}ML_n + \mathrm{O^*} \rightarrow \|{-}M^*\ (\text{ or } \|-M\mathrm{O^*})\ +\ \mathrm{CO_2 + H_2O}. \tag{14}$$

The combustion naturally forms metal oxides on the surface. However, for the noble metals, their oxides are either unstable or can be efficiently reduced by the metal precursor in the subsequent half-cycle [50, 51]. Therefore, this approach has also been applied to the ALD of Ru [50, 52], Os [53], Rh [54, 55], Ir [56, 57], Pd [58, 59], Pt [60, 61], and Au [62, 63] metals.

The oxidation approach can also be applied to deposit metal oxides with high oxidation states. Some metal precursors have low oxidation states for their metal ions, and by using this oxidation approach, the oxidation states of the metals can be increased in the deposited oxides. One example is the ALD of In_2O_3 from cyclopentadienyl indium(I) (InCp), where indium is monovalent in the precursor and trivalent in the target oxide. To achieve the oxidation, H_2O and O_2 can together be used as the oxygen sources [64]. In this process, the surface –Cp groups are first released by H_2O, with no change on the indium oxidation state, and then O_2 oxidizes the indium ions from $+1$ to $+3$ (figure 3(a)). Another example is the ALD of SnO_2 from N^2,N^3-di-tert-butyl-butane-2,3-diamido-tin(II) and H_2O_2 [65, 66]. In this case, the stannylene molecule is a π-acid, and it

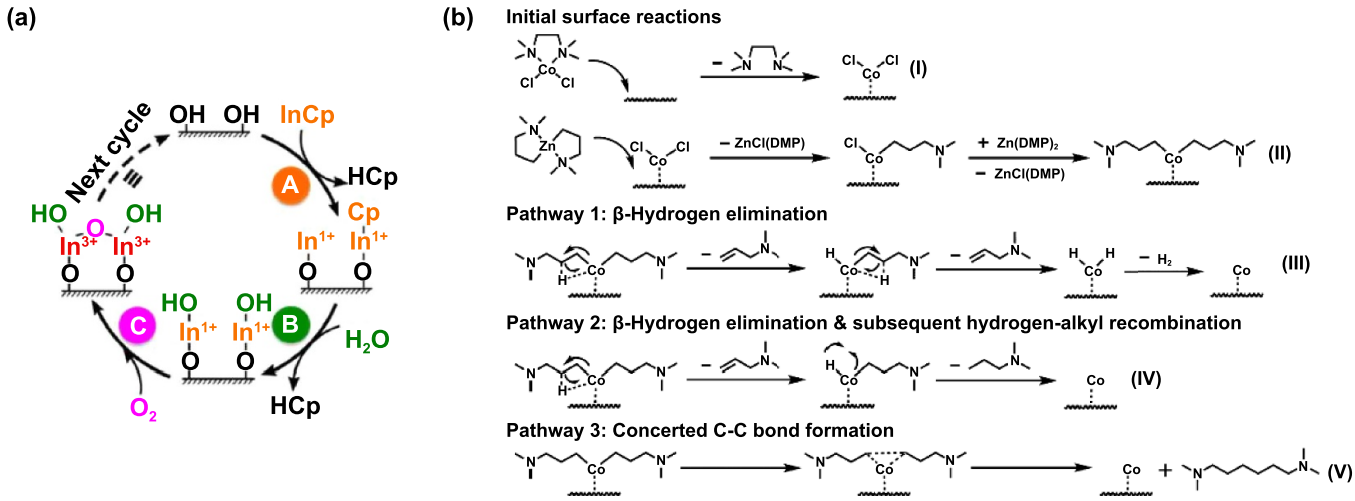

Figure 3. Schemes of the oxidation and reduction mechanisms. (a) Oxidation mechanism for the ALD of In_2O_3 using InCp, H_2O, and O_2. Reprinted with permission from [64]. Copyright (2017) American Chemical Society. (b) Proposed reaction pathways (reduction mechanism) for the ALD of Co using $CoCl_2$(TMEDA) and $Zn(DMP)_2$. Reprinted with permission from [39]. Copyright (2021) American Chemical Society.

can associate to a surface –OH group in the tin precursor half-cycle. Upon the H_2O_2 dose, the ligand bonded to the tin atom is first displaced by a hydroxyl group from H_2O_2, and then additional H_2O_2 can further oxidize tin(II) to tin(IV) via oxidative addition. It is worth noting that the final oxidation state depends on the exposure of the oxidant.

2.4. Reduction mechanism

The reduction mechanism is commonly involved in the ALD of metals, where the surface groups bonded to the metal atoms are removed by a reducing agent. H_2 gas is a typical reducing agent, and it has been used in depositing a variety of metals [67–73]. The corresponding reductive mechanism involves the elimination of the surface ligands by H_2, as expressed in the following:

$$\| - ML_n + \ n/2\ \mathrm{H_2} \rightarrow \| - M^* \ + \ n\ \mathrm{HL}\ (\mathrm{g})\,. \qquad (15)$$

Similarly, nitrogen-containing reducing agents, such as NH_3 [71, 72, 74] and N_2H_4 [75], can also be used to deposit metal films, but nitrogen impurities are often induced. Alcohols can also be used with metal β-diketonates to deposit the transition metals of Ni [76], Cu [77], and Pd [78]. During these processes, the alcohols produce reductive hydrogen radicals via the dehydrogenation reactions as catalyzed by the transition metal surfaces [79, 80].

Another type of the reduction mechanism is related to the reductive elimination of the surface species. For instance, the reduction of Ti upon the adsorption of the $TiCl_4$ was reported in previous literature, but the involved mechanisms were not shown [81]. More evidence of the reductive elimination was found for the metal amides. It was proposed that the ALD of TiN using $Ti(NMe_2)_4$ involves the reductive elimination of the dimethylamino ligands to afford hydrazine [82],

$$2\,\| - \mathrm{Ti(NMe_2)_2} \rightarrow 2\| - \mathrm{Ti\,(NMe_2)} \ + \ \mathrm{Me_2NNMe_2\,(g)}\,, \qquad (16)$$

and the oxidation state of Ti changes from +4 to +3. The reductive elimination may also be accompanied with the β-hydrogen elimination to produce amine [82, 83]. As another example, in the aforementioned ALD process to deposit Cu (equations (7) and (8)), the intermediate surface ethyl groups are unstable and prone to the coupling to form the pure metal and volatile butane. A similar reductive elimination mechanism was suggested for the ALD of Co from $CoCl_2$(TMEDA) (TMEDA = *N,N,N′,N′*-tetramethylethylenediamine) and $Zn(DMP)_2$ (DMP = dimethylaminopropyl). According to the DFT calculation, the reductive elimination pathway was most viable through the concerted C–C bond formation, and the β-hydrogen elimination may also take place in the metal reduction (figure 3(b)) [39]. However, many proposed pathways of the reductive elimination are not explicitly proved, and further investigations are still needed.

2.5. Plasma-assisted ALD

Plasma is sometimes used to assist the ALD, and such method is also known as plasma-assisted ALD (PALD). PALD utilizes the energetic species of radicals, ions, and electrons generated from the plasma as the reactants, and using the plasmas of O_2, NH_3, H_2S, and H_2, one can deposit oxides, nitrides, sulfides, and metals, respectively. The surface chemistry mechanisms of PALD are significantly complex, and they may consist of multiple mechanisms as discussed above. Owing to the high reactivity of the species from the plasmas, the surface reactions in PALD are usually easier to reach completion, and many low-reactivity metal precursors can be employed for PALD even at a low deposition temperature. For instance, with the O_2 plasma, some precursors (e.g. cyclopentadienyls and β-diketonates) that show low reactivity with H_2O or O_2

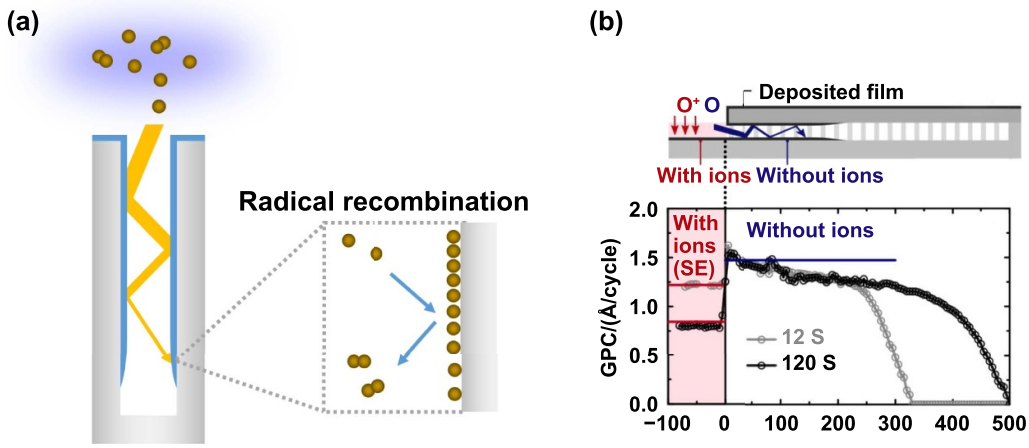

Figure 4. Plasma-assisted ALD. (a) Schematic illustration of the radical recombination on the walls of the trench. (b) Spatial distribution of the PALD SiO_2 film thickness in a cavity, using different plasma exposures. The unit of the *x*-axis is micrometer. Reprinted from [89], with the permission of AIP Publishing.

can also be used to deposit oxides; with the H_2 plasma, the hydrogenation of the precursor ligands is more efficient, which is helpful to deposit dense pure metal films. The diversity of the plasma also offers more tunability of the film composition. For instance, the N element can be incorporated into the films by adding N_2 to the O_2 plasma straightforwardly [84, 85]. As another example, Guo and Wang [86] employed the H_2S plasma to deposit the sulfur-rich phases of the metal pyrites of FeS_2, CoS_2, and NiS_2. The energetic reactive species in the plasma provided sufficient driving force to form the dimeric S–S moiety in the pyrites, which can hardly be achieved by the thermal ALD using molecular H_2S. On the other hand, the radicals and electrons may also activate additional reactions on the surface. For instance, the electrons from plasma can promote the desorption of hydrogen from the $–NH_2$ species on the surface [87]. It is worth noting that the presence of large amounts of gas-phase and surface species make the chemistry of PALD very complex. In some cases of using two reactant gases in the plasma, new molecules can be formed through gas-phase reaction or recombination [88]; the byproducts from the surface reactions may also be dissociated by the plasma when they are desorbed from the surface [17].

Notably, a concern about PALD is that the radicals generated from the plasma are prone to recombine. Therefore, compared to thermal ALD, the conformality of the film coating on high-aspect-ratio trench structures is sometimes compromised in PALD, owing to the severe radical recombination on the walls of the trench, as shown in figure 4(a). In addition to radicals, of which the diffusion is isotropic, the charged ions also play an important part in the PALD process. The charged ions can be accelerated in the direction perpendicular to the substrate surface within the plasma sheath, thus leading to the ion bombardment [90]. The ion energy is susceptible to the mean free path, plasma sheath thickness, and applied bias. Additional energy can be provided to the substrate surface, which may enhance the surface reaction or diffusion. Also, a recent study showed that the ions with low energy under mild plasma condition could significantly influence the deposition. As shown in figure 4(b), conformal deposition in the cavity with a high aspect ratio of 900:1 was successfully achieved [89]. However, in the area exposed to the anisotropic ions, a comparatively lower growth rate was observed. These results show the promise of using radicals to achieve good film step coverage. More methods, such as substrate biasing [91] and waveform tailoring [92], have been studied to modulate the ion energy. These methods are promising for better control of the film properties (e.g. crystallinity and conformality).

2.6. Nonideal factors

Despite numerous merits of ALD to fabricate high-quality films, a large fraction of the reported ALD processes do involve nonideal issues, and therefore, a good understanding of these issues is critical for better film quality control. To this end, we elaborate some typical nonideal factors in ALD as follows, including nucleation delay, byproduct adsorption, ligand decomposition, agglomeration, and ion diffusion.

2.6.1. Nucleation delay. The initial nucleation of the film growth is an important aspect in ALD. As shown in figure 5(a), the nucleation delay is a phenomenon that the apparent film growth rate was significantly slower in the initial stage than that in the later steady-growth stage, owing to a limited number of the nuclei formed initially on the surface. In ALD, the precursor usually needs to react with a functional group on the surface, and therefore lacking such functional groups on the initial substrate surface would result in significant nucleation delay for the film growth. For an inert surface, the nucleation usually starts from the surface defects, and in such cases, the initial ALD film growth is usually nonuniform and tends to form discontinuous islands [93]. These islands continue to

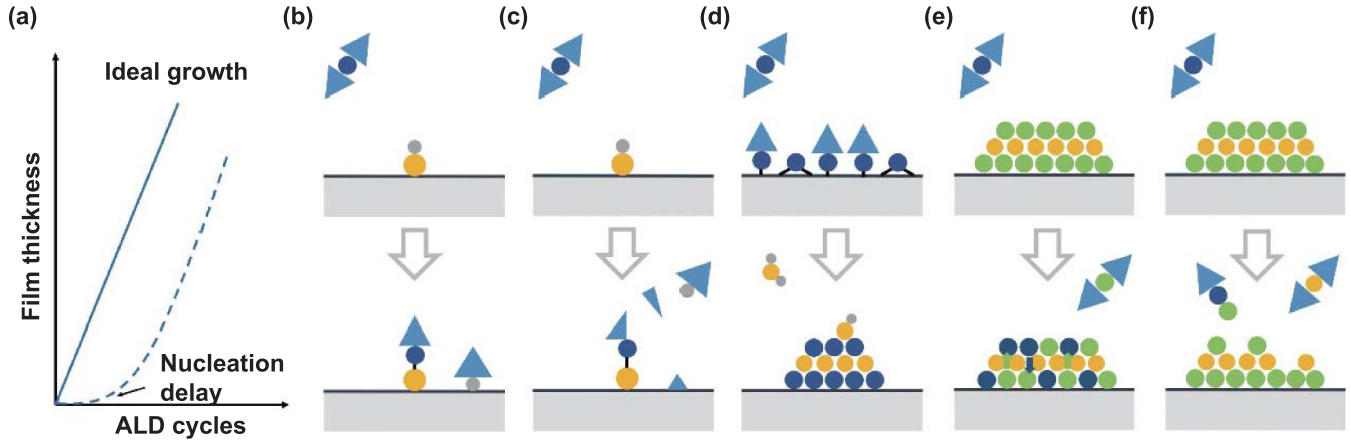

Figure 5. Schematic illustration of the typical nonideal factors in ALD: (a) nucleation delay, (b) byproduct adsorption, (c) ligand decomposition, (d) agglomeration, (e) ion diffusion, and (f) etching effect.

grow in the follow-up ALD process and eventually coalescence to form a continuous film. It is worth noting that the nucleation delay is quite common for the ALD of oxides on the inert H-terminated silicon [94, 95]. Another example is the ALD of the platinum group metals on inert substrates using O_2 as the co-reactant [53, 96]. The lack of the activation of O_2 on the initial substrate hinders the chemisorption of metal precursor through oxidation mechanism, which results in the nucleation delay. Notably, because of the steric hindrance of the organic ligands, not all the active surface sites can react with the precursor molecule in each ALD cycle, and therefore, an ALD cycle usually affords less than one monolayer of the deposited material [35, 97, 98], and the island growth is sometimes inevitable.

2.6.2. Byproduct adsorption. In an ideal ALD process, the byproducts from the surface reactions should be sufficiently volatile to be completely liberated from the surface; however, this is not always the case in actual ALD processes. For instance, Zhao *et al* [99] found that for the ALD of NiS_x from bis(*N,N′*-di-*tert*-butylacetamidinato)nickel(II) [$Ni(amd)_2$] and H_2S, the reaction byproduct (*N,N′*-di-*tert*-butylacetamidine, Hamd) was not released from the surface during the H_2S half-cycle but formed a nonvolatile acid-base complex with the sulfhydryl on the surface:

$$\| - \mathrm{Ni} - \mathrm{amd} + \mathrm{H_2S} \rightarrow \| - \mathrm{Ni} - \mathrm{SH} \ldots \mathrm{Hamd}. \qquad (17)$$

Another common case is the ALD process with metal chlorides and H_2O [100]. The released HCl during the ligand-exchange can further react with the surface hydroxyl groups and even corrode the deposited films. Generally, the adsorbed byproducts can occupy the reactive sites on the surface (figure 5(b)) and therefore reduce the film growth rate [5]. Also, the adsorbed byproducts may be trapped in the deposited films or at the interfaces as impurities [101].

2.6.3. Ligand decomposition. The ligands on the surface are not always stable, and they may decompose into small fragments during ALD. As shown in figure 5(c), the afforded fragments may still be removable by the co-reactants in the follow-up half-cycle, but if the removal is not complete, the residual fragments may be trapped in the film and become impurities. More importantly, the ligand decomposition may result in the loss of the self-limiting nature of ALD; in fact, as a consequence of the ligand decomposition, CVD-like growth behaviors were often observed at high deposition temperatures. The decomposition of the surface ligands is often a temperature-dependent multi-step process, and therefore, understanding the details of the decomposition process is highly important for the ALD process development and engineering. The decomposition process can be investigated by studying the thermolysis behavior of a precursor on a solid surface. For instance, Zhao *et al* [102] utilized *in situ* XPS to investigate the surface thermolysis behavior of a nickel precursor of $Ni(amd)_2$ on SiO_x. The surface amidinate moiety from the nickel precursor was found to decompose at 250 °C, which implied an upper temperature limit for the use of the $Ni(amd)_2$ precursor for ALD. Indeed, the corresponding *ex situ* ALD experiments did show that the C and N impurity levels substantially increased if the deposition temperature was beyond 250 °C [103].

2.6.4. Agglomeration. During ALD, small deposits can agglomerate to form nanosized clusters or particles on the surface. The agglomeration can be induced by the surface atom diffusion or Ostwald ripening [104]. This phenomenon is often observed in the ALD of noble metals, and it has been extensively applied to the engineering of chemical catalysts at nanoscale [67, 104, 105]. In another case, Zhao and Wang [106] proposed a reaction-agglomeration scheme (figure 5(d)) for the initial ALD growth of NiS_x on SiO_x. In that scheme, the nickel precursor first reacted with the SiO_x surface to afford Ni–O bonds, and the afforded Ni–O bonds

converted to NiS_x in the subsequent H_2S half-cycle with spontaneous agglomeration to form NiS_x clusters. This agglomeration could re-expose the SiO_x surface and allow for it to further react with the nickel precursor in the follow-up ALD cycle. Therefore, the agglomeration issue is highly important for the growth of ultrathin films by ALD.

2.6.5. Ion diffusion. In some ALD processes, the diffusion of the ions in the substrates or deposited films cannot be overlooked. For instance, Zhu *et al* [107] found that the ALD growth of NiS_x on a Co_9S_8 film could significantly reduce the Co amount in the Co_9S_8 film, and this phenomenon was because of the simultaneous occurrence of the gas–solid metal exchange reaction as

$$\|-\mathrm{Co}^* + \mathrm{Ni(amd)_2\,(g)} \rightarrow \| - \mathrm{Ni}^* + \mathrm{Co(amd)_2\,(g)}, \quad (18)$$

together with the fast diffusion of the metal ions inside the Co_9S_8 film (figure 5(e)). The similar gas–solid metal exchange reactions were also observed in the ALD growth of Al_2O_3 on a ZnO film [108, 109]. This effect can be very important for the ALD of multi-element compounds (e.g. ternary or quaternary compounds) because the most common approach to deposit the multielement compounds is to alternately deposit binary compounds in supercycle manner. In another case, significant out-diffusion of the oxygen ions from the substrate was observed for the ALD of Al_2O_3 on the Sn-doped In_2O_3 (ITO) substrate [110]. The out-diffusion of the oxygen ions resulted in non-self-limited chemisorption of TMA, which substantially enhanced the initial growth of Al_2O_3 on ITO. Therefore, the ion diffusion effect should be carefully considered if the involved ions are possibly mobile in the substrates or deposited films.

2.6.6. Etching effect. The etching effect may occur during the film deposition. This effect is common in PALD, in which the energetic ions from plasma can sputter off the films and thus etch the materials [91, 92]. The etching effect mainly depends on the plasma power and exposure in PALD, and therefore, the plasma parameters should be carefully tuned when depositing films. The etching effect may also occur through the chemical reaction to form volatile products (figure 5(f)), and a well-known example is the pulsing of $Al(CH_3)_3$ on the AlF_3 film surface. $Al(CH_3)_3$ would react with AlF_3 through the ligand-exchange to form the volatile $AlF(CH_3)_2$ [111]:

$$\mathrm{AlF_3} + 2\mathrm{Al(CH_3)_3} \rightarrow 3\mathrm{AlF(CH_3)_2}, \quad (19)$$

and AlF_3 is removed during the reaction. It is worth noting that the self-limiting etching of Al_2O_3 can be achieved by the fluorination followed by the etching reaction, and this strategy is extensively used in atomic layer etching [112, 113].

3. Precursor chemistry of ALD

Generally, the ALD precursors should be of sufficient volatility, thermal stability, and self-limiting reactivity. The volatility is a prerequisite for all vapor-phase thin-film deposition techniques, and for ALD, the precursors are desired to have a saturated vapor pressure of >0.1 Torr. To afford sufficient vapor pressure, the precursor compounds are often needed to be heated during ALD, and therefore, the precursors should be of sufficient thermal stability. The thermal stability is also important to avoid the precursor decomposition on the substrate surface, as otherwise, it would lead to the loss of the self-limiting growth. The precursors should also be of sufficient reactivity with the surface groups, and as discussed in the previous section, the surface chemical reactions should be self-limiting, as otherwise, the deposition would be CVD-like. Over the years, many efforts have been devoted to engineer the precursor molecule structures to achieve the desired attributes for the ALD applications. For instance, to enhance the precursor volatility, the precursor molecules often adopt organic ligands with alkyl terminals to reduce the intermolecular interactions. To enhance the precursor thermal stability, one can use bidentate ligands to form chelated structures with the metal ions. Table 1 summarizes some typical categories of the metalorganic compounds that have been often used as the precursors in ALD, including metal halides, alkyls, cyclopentadienyls, alkoxides, β-diketonates, amides, amidinates, and heteroleptic precursors. This table is not aimed to list all the precursors, and some others include metal diazadienyls [114–118] and carbonyls [119–124], which are somewhat less commonly used. A more comprehensive survey can be found in an online ALD database [125].

3.1. Metal halides

Metal halides, such as chlorides and fluorides, have been used as the precursors since the early days of ALD. The halides usually have a good thermal stability, which is desirable for ALD. As an example, $TiCl_4$ has a long history of use in the IC manufacturing for the deposition of TiN [201], which is the electrode material of DRAM. Because DRAM has a 3D structure with high aspect ratio, the excellent conformality feature of ALD is indispensable for this application. However, the deposition temperature was often high (>300 °C), and the deposited films usually contained halogen impurities. As another example, $HfCl_4$ can be used with H_2O to deposit HfO_2, which is a high-k dielectric material for CMOS devices. In the deposited HfO_2 films, the chlorine impurity was reported to be ca. 5% when the deposition temperature was 225 °C, and increasing the deposition temperature to 500 °C could significantly reduce the chlorine level [133, 202]. Also, the nucleation delay was observed in this process, and the HfO_2 films grew as islands on the H-terminated Si surfaces at the initial stage, which could cause large electrical leakage for the gate dielectric applications. To this end, additional surface treatments many be needed to remedy this issue. The silicon surface

Table 1. Summary of the ALD metal precursors and film deposition examples.

Precursor		Film deposition example				
Category	Formula	Material	Co-reactant	Deposition temperature (°C)	Growth rate (Å/cycle)	References
Halides	$TiCl_4$	TiO_2	H_2O	200–600	0.35–0.45	[126]
	$NbCl_5$	NbN_x	NH_3	300–400	0.16	[127]
	$TaCl_5$	Ta	H_2 plasma	250–400	1.67	[128]
	MoF_6	Mo	Si_2H_6	90–150	6–7	[36]
		MoS_2	H_2S	700	0.22	[129]
	WF_6	W	Si_2H_6	150–325	2.5	[130]
		WN_x	NH_3 plasma	315–375	2.0	[131]
	$ZrCl_4$	ZrO_2	H_2O	500	0.53	[132]
	$HfCl_4$	HfO_2	H_2O	500	0.5	[133]
	$InCl_3$	In_2Se_3	$(Et_3Si)_2Se$	295	0.55	[134]
	$GaCl_3$	GaN	NH_3	550	2.0	[135]
	$ZnCl_2$	ZnSe	$(Et_3Si)_2Se$	400	0.55	[134]
	ZnI_2	ZnS	H_2S	300–450	0.45	[136]
Alkyls	$Zn(C_2H_5)_2$	ZnO	H_2O	130–175	1.9	[137]
	$Cd(CH_3)_2$	CdO	H_2O	150	2	[138]
	$Al(CH_3)_3$	Al_2O_3	H_2O	77–277	1.0–1.1	[139]
	$Ga(CH_3)_3$	Ga_2O_3	O_3	200–375	0.52	[140]
	$In(CH_3)_3$	In_2O_3	O_3	100–200	0.46	[141]
	$Sn(CH_3)_4$	SnO_2	N_2O_4	250–290	2.5	[142]
Cyclopentadienyls	$Mg(EtCp)_2$	MgO	H_2O	150	1.42	[143]
	$Sr(PrMe_4Cp)_2$	SrO	$H_2O + O_2$	250–350	0.4	[144]
	$ScCp_3$	Sc_2O_3	H_2O	250–350	0.75	[145]
	$Y(MeCp)_3$	Y_2O_3	H_2O	200–275	1.2	[146]
	$Mn(EtCp)_2$	MnO	H_2O	100	1.2	[147]
	$FeCp_2$	FeO_x	O_2	350–500	1.4	[148]
	$CoCp_2$	Co_3O_4	O_3	150–280	0.41	[149]
	$NiCp_2$	NiO	O_3	230	0.92	[150]
	$Ru(EtCp)_2$	Ru	O_2	270	1.5	[151]
	InCp	In_2O_3	O_3	200–450	1.2–1.4	[152]
Alkoxides	$Li(O^tBu)$	Li_2O	H_2O	225–300	0.12	[153]
	$Ti(O^iPr)_4$	TiO_2	H_2O	90–200	0.35	[154]
	$Zr(O^tBu)_4$	ZrO_2	H_2O	150–250	1.3	[155]
	$Hf(O^tBu)_4$	HfO_2	O_3	300	0.4	[156]
	$VO(O^iPr)_3$	VO_x	O_2 plasma	50–200	0.5	[157]
	$Ta(OEt)_5$	Ta_2O_5	H_2O	250–325	0.4	[158]
	$Al(O^iPr)_3$	Al_2O_3	H_2O	140–300	1.2–1.8	[159]
β-diketonates	$[Mg(thd)_2]_2$	MgO	H_2O_2	325–425	0.10–0.14	[160]
	$Ca(thd)_2$	$CaCO_3$	O_3	200–350	0.45	[161]
	$Sc(thd)_3$	Sc_2O_3	O_3	335–375	0.125	[145]
	$Fe(thd)_3$	FeO_x	O_3	186	0.11	[162]
	$Co(thd)_2$	Co_3O_4	O_3	114–307	0.2	[163]
	$Ni(acac)_2$	NiO	O_3	250	0.3–0.5	[70]
	$Cu(acac)_2$	Cu	H_2 plasma	140	0.18	[164]
	$Ru(thd)_3$	Ru	O_2	250	0.15	[165]
	$Rh(acac)_3$	Rh	O_3	200–220	0.42	[55]
	$Pd(hfac)_2$	Pd	O_3	180–220	0.22	[55]
	$Ir(acac)_3$	Ir	$O_2 + H_2$	200	0.2	[166]
	$Pt(acac)_2$	Pt	O_3	140	0.5	[167]
	$La(thd)_3$	La_2O_3	O_3	250	0.35	[168]
	$Ce(thd)_4$	CeO_2	O_3	175–250	0.32	[169]

(Continued.)

Table 1. (Continued.)

Precursor		Film deposition example				
Category	Formula	Material	Co-reactant	Deposition temperature (°C)	Growth rate (Å/cycle)	References
	$Nd(thd)_3$	Nd_2O_3	O_3	310	0.43	[170]
	$Sm(thd)_3$	Sm_2O_3	O_3	300	0.35	[170]
	$Eu(thd)_3$	Eu_2O_3	O_3	300	0.31	[170]
	$Gd(thd)_3$	Gd_2O_3	O_3	300	0.30	[170]
	$Dy(thd)_3$	Dy_2O_3	O_3	300	0.30	[170]
	$Er(thd)_3$	Er_2O_3	O_3	300	0.19	[171]
	$Lu(thd)_3$	Lu_2O_3	O_3	300	0.18	[171]
Alkylamides	$Ti(NMe_2)_4$	TiO_2	H_2O	150	0.58	[154]
	$Zr(NMe_2)_4$	ZrO_2	H_2O	100	1.0	[172]
	$Hf(NMe_2)_4$	HfO_2	H_2O	205–235	0.72	[173]
	$V(NMe_2)_4$	VO_x	H_2O	50	0.32	[174]
	$Ta(NMe_2)_5$	Ta_2O_5	H_2O	200–250	0.85	[175]
	$Ga_2(NMe_2)_6$	Ga_2O_3	H_2O	170–250	1.0	[176]
	$Sn(NMe_2)_4$	SnO_2	H_2O_2	50–300	1.2	[177]
	$Si(NMe_2)_4$	SiO_2	H_2O_2	150–550	0.8–1.8	[178]
	$Ge(NMe_2)_4$	GeO_2	O_3	180–230	0.45	[179]
Amidinates	$Ca(^iPr_2FMD)_2$	CaS	H_2S	150–280	0.87	[180]
	$Sc(^iPr_2AMD)_3$	Sc_2O_3	H_2O	290	0.3	[181]
	$Y(^iPr_2AMD)_3$	Y_2O_3	H_2O	150–280	0.8	[182]
	$V(^iPr_2AMD)_3$	VO_x	O_3	190	1.57	[183]
	$Mn(^tBu_2AMD)_2$	MnO_x	H_2O	175–250	2.1	[184]
	$Fe(^tBu_2AMD)_2$	FeS_2	H_2S plasma	200	1.06	[86]
	$Co(^iPr_2AMD)_2$	Co_9S_8	H_2S	80–165	0.27	[185]
	$Ni(^tBu_2AMD)_2$	NiS_x	H_2S	200	0.15	[99]
	$[Cu(^iPr_2AMD)]_2$	Cu	H_2 plasma	50–100	0.7	[186]
	$In(^iPr_2AMD)_3$	In_2O_3	H_2O	150–275	0.55	[187]
	$Sn(^iPr_2FMD)_2$	SnO	H_2O	140	0.82	[188]
	$La(^iPr_2AMD)_3$	La_2O_3	H_2O	300	0.9	[73]
	$Ce(^iPr_2AMD)_3$	CeO_2	O_3	220–255	2.8	[189]
	$Pr(^iPr_2AMD)_3$	PrO_x	H_2O	200–315	1.3	[190]
	$Gd(^iPr_2AMD)_3$	$GdScO_3$	H_2O	310	1.0	[191]
	$Er(^tBu_2AMD)_3$	Er_2O_3	O_3	225–300	0.37–0.55	[192]
	$Lu(Et_2FMD)_3$	Lu_2O_3	H_2O	300	1.2	[193]
Heteroleptic	$[Al(CH_3)_2(O^iPr)]_2$	Al_2O_3	O_2 plasma	150–250	0.85	[194]
	$ZrCp_2Cl_2$	ZrO_2	O_3	275–350	0.53	[195]
	$HfCp_2Cl_2$	HfO_2	O_3	325–400	0.54	[196]
	$TiCp(NMe_2)_3$	TiO_2	O_3	250–300	1.0	[197]
	$Y(^iPrCp)_2(^iPr_2AMD)$	Y_2O_3	H_2O	225	0.8	[198]
	$Pr(^iPrCp)_2(^iPr_2AMD)$	Pr_2O_3	H_2O	200	1.5	[198]
	$Gd(^iPrCp)_2(^iPr_2AMD)$	Gd_2O_3	H_2O	200	0.75	[198]
	$Dy(^iPrCp)_2(^iPr_2AMD)$	Dy_2O_3	H_2O	200	0.8	[198]
	$La(^iPrCp)_2(^iPr_2AMD)$	La_2O_3	O_3	200	0.5	[199]
	$CoCp(^iPr_2AMD)$	Co	NH_3 plasma	200–250	0.5	[200]

Cp = cyclopentadienyl; thd = 2,2,6,6-tetramethylheptane-3,5-dionato; acac = acetylacetonato; hfac = 1,1,1,5,5,5-hexafluoro-acetylacetonato; AMD = acetamidinato; FMD =formamidinato.

can be oxidized or nitrided to provide enough surface groups, which are typically reactive with the precursor [203, 204].

On the other hand, except for a few halides, such as WF_6, which is a gas at room temperature, the majority of the metal halides are not quite volatile and therefore require high-temperature heating to produce sufficient vapor for ALD. For example, $InCl_3$ and CuCl need to be heated to 275 °C and 340 °C, respectively, for ALD [205, 206]. In addition, the reaction byproducts of the halides include corrosive HF or HCl, which may further etch the substrates and deposited films, thereby deteriorating the uniformity and conformality of the ALD films. For instance, WF_6 and H_2 can be used to deposit tungsten metal, and the tungsten metal is used for the local interconnects in ICs. However, the HF generated by the ALD

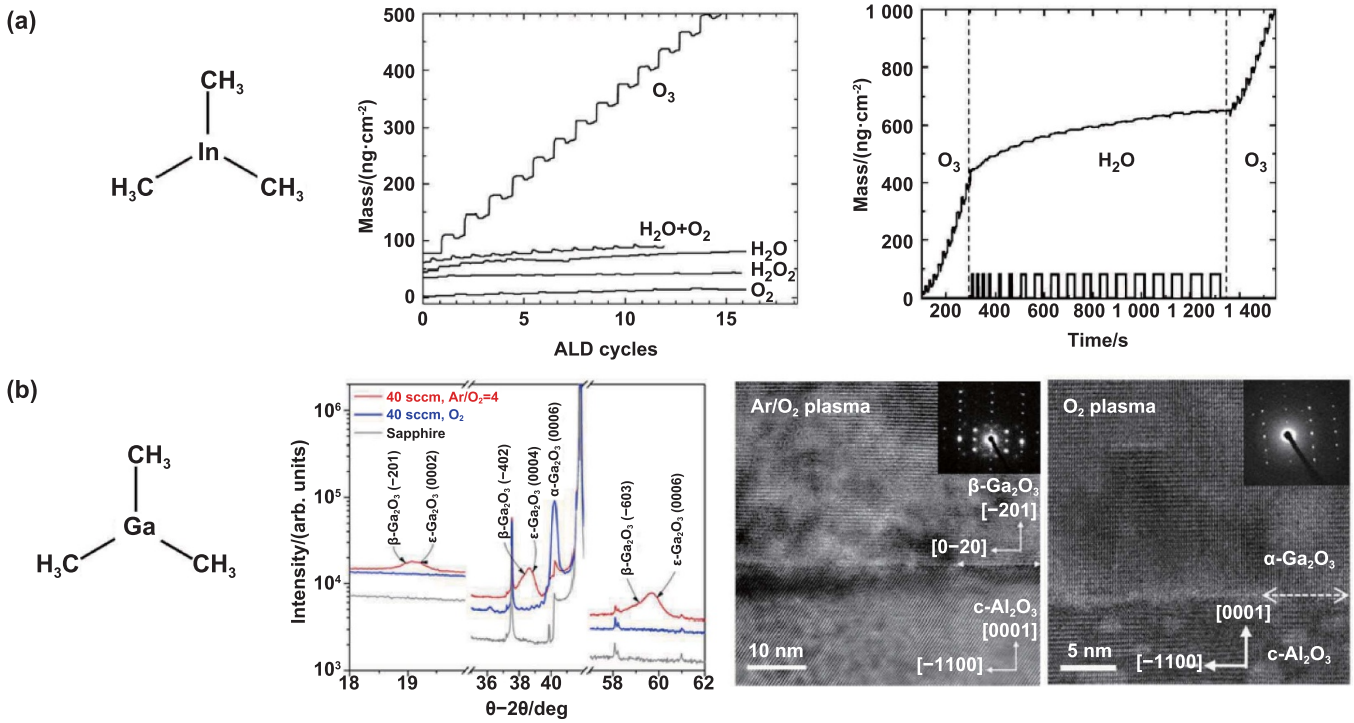

Figure 6. ALD from metal alkyls. (a) ALD of In_2O_3 from $In(CH_3)_3$ and ozone. Reprinted with permission from [141]. Copyright (2016) American Chemical Society. (b) ALD of Ga_2O_3 from $Ga(CH_3)_3$ and ozone. Reprinted with permission from [218]. Copyright (2020) American Chemical Society.

process of WF_6 and H_2 can corrode the SiO_2 dielectrics and cause electrical shorting between devices [207]. Despite of these issues, the halide precursors still have a significant role in manufacturing, and one of the most important considerations is their low cost.

3.2. Metal alkyls

Several metal alkyls are well-known for their excellent properties as ALD precursors, such as $Al(CH_3)_3$ and $Zn(C_2H_5)_2$. $Al(CH_3)_3$ is a typical metal alkyl precursor, which has widely used and comprehensively studied. $Al(CH_3)_3$ is highly volatile and can be used at room temperature for ALD. $Al(CH_3)_3$ is also highly reactive and can be used with H_2O [33, 35], H_2O_2 [208], O_3 [209, 210] and O_2 plasma [211] to deposit Al_2O_3. The involved gas–solid surface reactions are efficient and self-limiting, although some methyl ligands could persist on the surface when the deposition is below 300 °C using H_2O as the co-reactant [34]. $Al(CH_3)_3$ can also be used to deposit the III–V compounds of AlN [212], AlP [213], and AlAs [214] with the use of NH_3, PH_3, and AsH_3 as the co-reactants, respectively. Similar to $Al(CH_3)_3$, $Zn(C_2H_5)_2$ is also a desirable precursor, and it has been used to deposit ZnO [137], ZnS [215], ZnSe [216], and ZnTe [217] with the use of H_2O, H_2S, H_2Se, and H_2Te as the co-reactants, respectively.

As for the heavier IIIA elements of gallium and indium, the corresponding alkyl compounds, such as $In(CH_3)_3$ and $Ga(CH_3)_3$, have been used in semiconductor industry for the CVD of III–V materials (e.g. InP, InAs, GaN, and GaAs). However, compared to $Al(CH_3)_3$, $In(CH_3)_3$ and $Ga(CH_3)_3$ are less reactive with H_2O, and therefore, a stronger oxidant, such as O_3 [140, 141] or O_2 plasma [218, 219], is often needed for the ALD of the oxides (figure 6(a)). Particularly, for the ALD of Ga_2O_3 from $Ga(CH_3)_3$ and O_2 plasma, the crystal phase of the deposited Ga_2O_3 films could be controlled by the gas composition (Ar-diluted O_2), flow rate, and pressure during the plasma step, together with the deposition temperature (figure 6(b)) [218]. $Sn(CH_3)_4$ is also a reported ALD precursor; but its reactivity with H_2O is low, and therefore, a strong oxidant co-reactant, such as N_2O_4, is needed to deposit SnO_2 [142].

It should be noted that although the abovementioned metal alkyls are successful for ALD, most of the other metal alkyls do not have sufficient volatility or thermal stability. Therefore, the use of metal alkyl precursors is still limited to only a few metals.

3.3. Metal cyclopentadienyls

Metal cyclopentadienyls (Cp) have been used in a large number of ALD processes, and many of these compounds are fairly stability. For instance, the metal cyclopentadienyls (and their derivatives) have been quite successful for the ALD of the IIA-element compounds. As an example, $MgCp_2$ has been used with H_2O to deposit MgO, and the film growth rate was reported to be ca. 1.5 Å/cycle at 150 °C [220]. Similarly, $Sr(^iPr_3Cp)_2$ and $Ba(Me_5Cp)_2$ have been used with H_2O to deposit $SrTiO_3$ [221] and $BaTiO_3$ [222], respectively, and these compounds have also been used with H_2S to deposit SrS and BaS [223]. Notably, in these cases, the Cp rings are

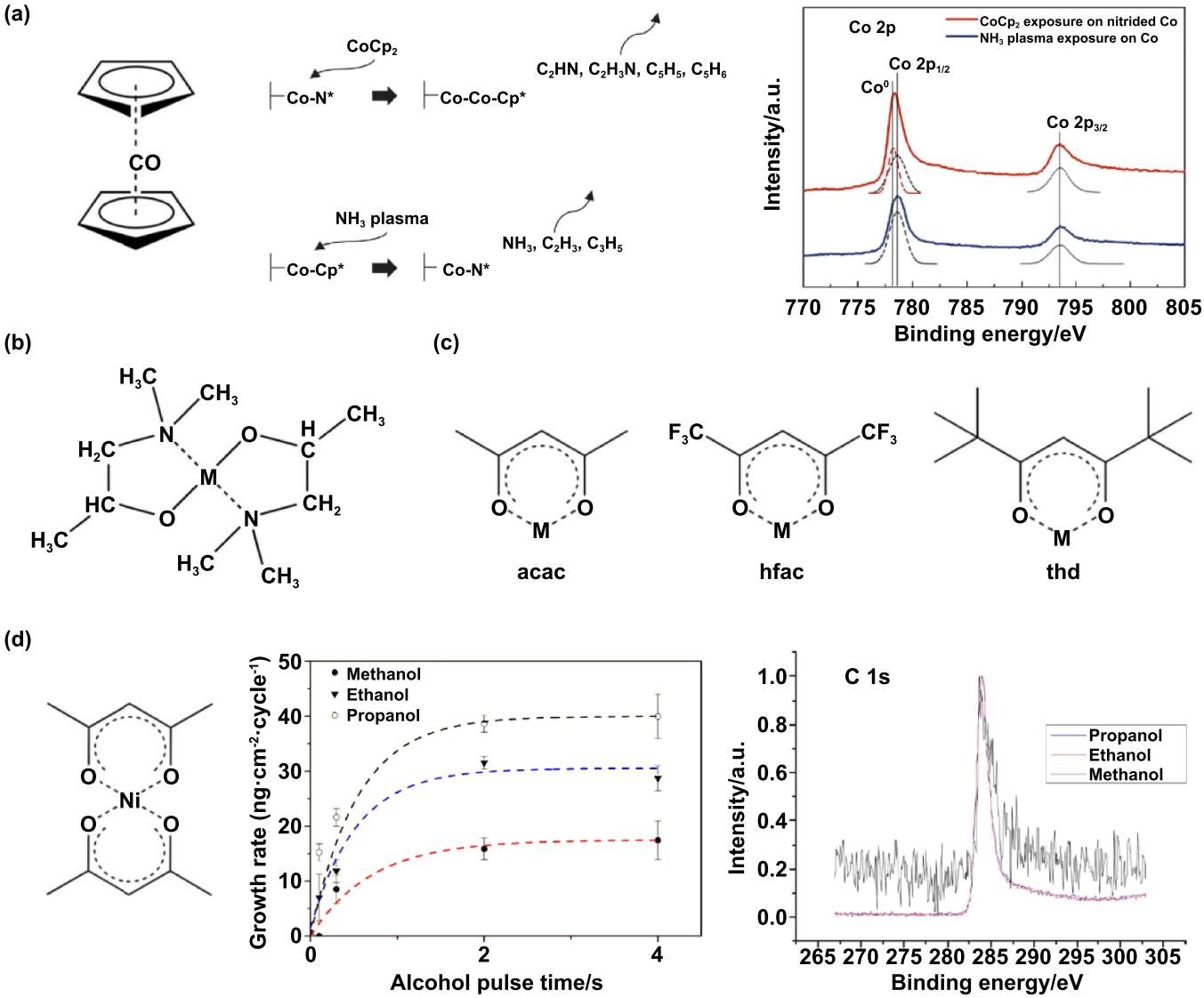

Figure 7. ALD from metal cyclopentadienyls, alkoxides and β-diketonates. (a) PALD of Co metal from $CoCp_2$ and NH_3 plasma. Reprinted from [230], Copyright (2017), with permission from Elsevier. (b) Chelated structure of $M(dmap)_2$. (c) Common β-diketonate ligands. (d) ALD of Ni from $Ni(acac)_2$ and primary alcohols. Reprinted with permission from [76]. Copyright (2014) American Chemical Society.

isopropyl- and methyl-substituted to prevent the oligomerization of these compounds, and this substitution strategy is fairly important for the bulky metal ions. Likewise, $La(^iPrCp)_3$ and $Ce(Me_4Cp)_3$ have been used for the ALD of La_2O_3 [224] and CeO_2 [225], respectively. A few late-3d-metal cyclopentadienyls, such as $CoCp_2$ [149, 226] and $NiCp_2$ [227, 228], have also been used for ALD, but they usually need a strong oxidant of O_3 or plasma (O_2, H_2, or NH_3 plasma) as the co-reactant to activate the surface reactions [229–231]. For instance, Co metal films can be deposited from $CoCp_2$ and NH_3 plasma, and in this process, the NH_3 plasma exposure generates a N-terminated surface, which can further react with $CoCp_2$ to form the Co–Co bonds and a series of volatile organic byproducts (figure 7(a)) [230]. As for the noble metals, their cyclopentadienyls (and derivatives) have been quite successful for ALD. Using O_2 as the reactant, Ru [151], Pt [232], and Ir [233] metals can be successfully deposited from their cyclopentadienyl precursors.

It is worth noting that it is sometimes difficult to completely remove the cyclopentadienyl ligands on the surface by a Brønsted-acid co-reactant, because the hydrogenation of cyclopentadienyl involves the breakup of its aromatic conjugation. Therefore, carbon residue could be an issue for the deposited films [234], and even for some cyclopentadienyl compounds, H_2O is not sufficiently reactive to serve as the co-reactant [152].

3.4. Metal alkoxides

Volatile metal alkoxides are also suitable ALD precursors. $Ti(O^iPr)_4$ is a representative example and has been used for the ALD of TiO_2. Using H_2O as the co-reactant, the ALD growth

rate of TiO_2 was found to be 0.2 Å/cycle at 150 °C–250 °C [235]. It is worth noting that the metal alkoxides can self-oligomerize in solution, and therefore, the deposition may be CVD-like at the low temperature near the precursor condensation point [236]. $Ti(OMe)_4$ is a more thermally stable precursor than $Ti(O^iPr)_4$, and the decomposition does not occur significantly until 350 °C; using H_2O as the co-reactant, the ALD growth rate for TiO_2 was 0.55 Å/cycle at 250 °C–325 °C [237]. In addition, $Ti(O^iPr)_4$ can be used in combination with $TiCl_4$ to directly deposit TiO_2 without using any other oxygen source. The reaction follows an alkyl-transfer mechanism, and the TiO_2 growth rate was 0.7 Å/cycle at 150 °C−250 °C [238].

Notably, the alkyl part of the alkoxide can be further engineered for the ALD applications. For instance, with an additional terminal dimethylamino group, the isopropoxide-derived ligand of dimethylamino-2-propoxide (dmap) can form chelated structures with metal ions (figure 7(b)), and the chelation can substantially enhance the stability of the formed metal–organic compounds. In this respect, $Cu(dmap)_2$ is a good example; as shown previously, $Cu(dmap)_2$ can be used with $Zn(CH_2CH_3)_2$ for the ALD of Cu metal [40]. In addition, it is worth noting that it is sometimes difficult to completely remove the surface alkoxide ligands during ALD, because the M–O bonds in the alkoxides are often quite strong. Therefore, oxygen and carbon impurities may be incorporated in the deposited films, and this issue can be critical for the ALD of pure metals [74].

3.5. Metal β-diketonates

Metal β-diketonates have been widely used as the ALD precursors. Many metals, including alkaline earth metals, transition metals and lanthanides, can form suitable β-diketonate compounds for the ALD applications. In a typical metal β-diketonate structure, the two ketone oxygen atoms coordinate to the center metal, forming a chelated six-member ring structure. The chelation can substantially enhance the compound thermal stability, and the side chains can be further tailored to promote the compound volatility. Common β-diketonate ligands include acetylacetonate (acac), 2,2,6,6-tetramethylheptane-3,5-dionate (thd), and 1,1,1,5,5,5-hexafluoroacetylacetonate (hfac) (figure 7(c)). The acac ligand is suited for small-size metals; whereas the bulky thd ligand is suited for large-size metals for preventing dimerization [239, 240]. The hfac ligand is a fluorine-substituted acac ligand, and the fluorine substitution can significantly enhance the compound volatility; however, it may also cause fluorine contamination in the deposited films.

Metal β-diketonates have been studied for the deposition of oxides [241–244], nitrides [245], sulfides [246–248], and metals [55, 59, 166, 167]. For the oxide deposition, owing to the stable chelated structures of the metal β-diketonates, the ALD processes usually need either high deposition temperature [249, 250] or a stronger oxidant, such as O_3 or O_2 plasma, as the co-reactant [241–244]. Also, pure nitrides and sulfides are not easy to achieve, because the surface β-diketonate ligands are difficult to be completely removed in these ALD processes [248, 251]. Noble metals, such as Rh [55], Pd [59], Ir [166], and Pt [167], can be deposited from the metal β-diketonates based on the combustion chemistry. In some cases, organic reducing agents, such as formalin [252], methanol [76], and hydroquinone [253], can be used with the metal β-diketonates to deposit metal films. For instance, Pd metal could be deposited from $Pd(hfac)_2$ and formalin, and the growth rate was found to be 0.35 Å/cycle at 200 °C [252]. As another example, Ni metal films could be deposited from $Ni(acac)_2$ with a primary alcohol at a temperature below 300 °C [76]. As shown in figure 7(d), three primary alcohols of ethanol, propanol, and methanol were evaluated, and methanol gave out the best results, as the deposited films were high-purity metallic Ni with low resistivity. In addition, the thd-based metal β-diketonates can also be used with TiF_4 or TaF_5 to deposit metal fluorides, such as MgF_2, CaF_2, and LaF_3 [254].

3.6. Metal amides

Metal amides generally have a high reactivity, and therefore, if they are volatile, they can be used for low temperature ALD (<100 °C). The low ALD temperature can allow for the films to grow on thermally unstable substrates, such as polymers, plastics, and photoresists [255]. As an example, $M(NMe_2)_4$, $M(NMeEt)_4$, and $M(NEt_2)_4$ (M = Hf, Zr) have been used as the hafnium and zirconium precursors to deposit ZrO_2 and HfO_2 [172]. $V(NMe_2)_4$ has been used with H_2O or O_3 to deposit VO_x films at 50 °C–200 °C (figure 8(a)) [256, 257]. All these precursors are highly volatile and reactive. When using H_2O as the co-reactant, the ALD surface reactions follow a proton-transfer ligand-exchange scheme, where the alkylamide ligand accepts a proton from the surface –OH, affording the alkylamine as the byproduct, while the metal ion bonds to the surface oxygen. This exchange reaction is highly exothermic, as the metal–oxygen bond is stronger than the metal–nitrogen bond and the amine is more basic than the alcohol. However, the thermal stability of the metal alkylamides is generally limited, and therefore, high deposition temperature may lead to the partial decomposition of the metal alkylamides and therefore increase the carbon and nitrogen impurity levels in the deposited films.

The thermal stability can be improved using a diamide ligand to form a chelated cyclic structure with the metal ion [258, 260]. As shown in figure 8(b), (*N,N′*-di-*t*-butyl-2-methylpropane-1,2-diamido)tin(II) has been used as the tin precursor for depositing SnS. Using H_2S as the co-reactant, the SnS growth rate was approximately 0.12 nm/cycle at the deposition temperatures of 75 °C–175 °C [258].

Metal amides have also been applied to the ALD of metal nitrides. Using $Ti(NEt_2)_4$ and NH_3 plasma, TiN films with a low resistivity of ca. 250 $\mu\Omega$ cm were deposited at 300 °C; however, higher carbon concentration was observed at lower deposition temperatures [261]. $Ta(NMe_2)_5$ was used with H_2 plasma to deposit TaN [201]. The TaN film growth rate was 0.56 Å/cycle at 225 °C, and the film electrical resistivity was 380 $\mu\Omega$ cm. Long H_2 plasma pulse time was found to be important to remove the carbon residue in the films. ALD of GaN was achieved by using $[Ga(NMe_2)_3]_2$ and NH_3 plasma

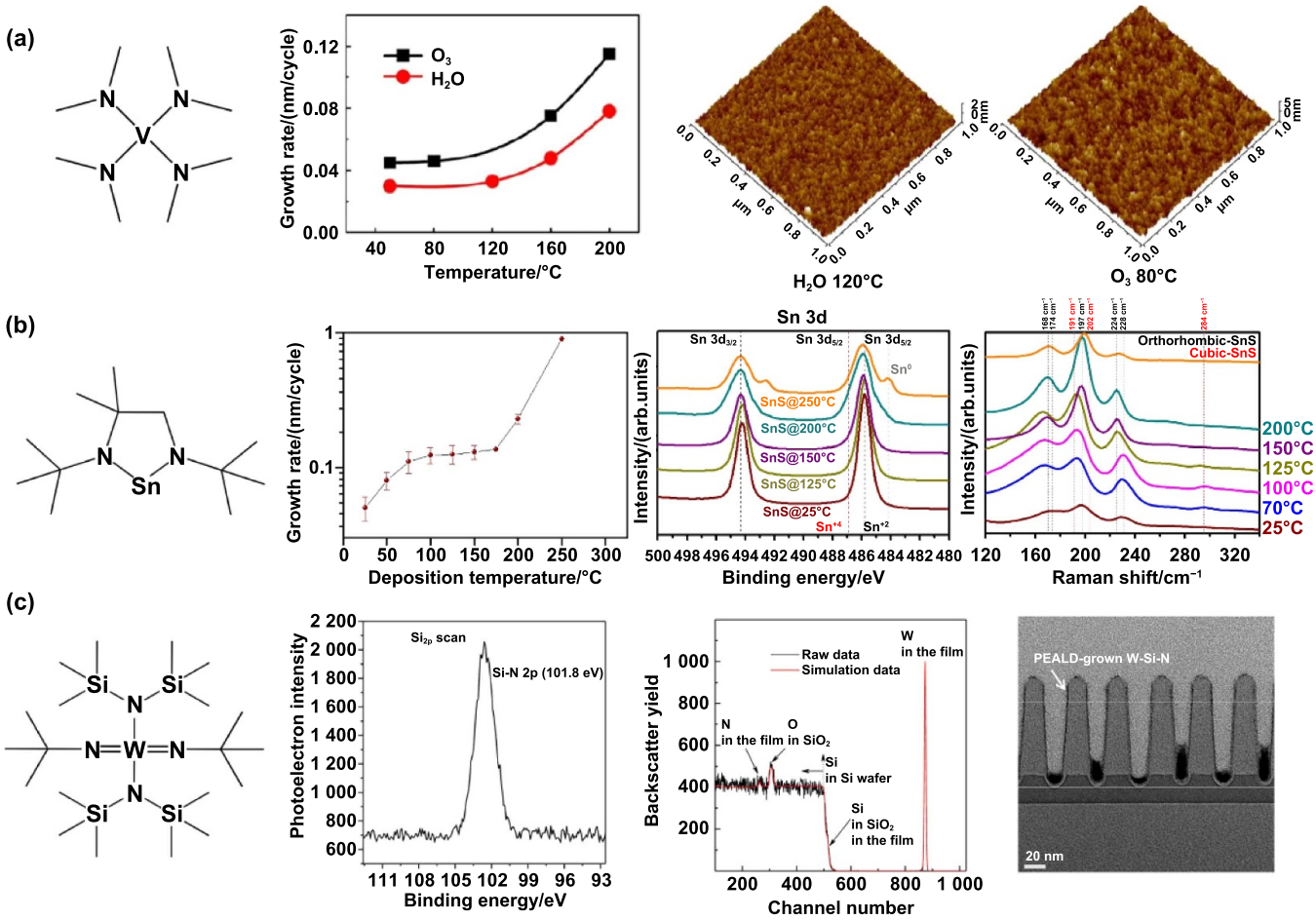

Figure 8. ALD from metal amides. (a) ALD of VO_x from $V(NMe_2)_4$ with the co-reactant of H_2O or O_3. Reprinted by permission from Springer Nature Customer Service Centre GmbH: Springer Nature, Journal of Materials Research [257], Copyright (2017). (b) ALD of SnS from (*N,N′*-di-*t*-butyl-2-methylpropane-1,2-diamido)tin(II) and H_2S. Reprinted from [258], Copyright (2021), with permission from Elsevier. (c) ALD of W_xSi_yN from $W(N^tBu)_2[N(SiMe_3)_2]_2$ and H_2 plasma. Reprinted with permission from [259]. Copyright (2015) American Chemical Society.

[262]. The self-limiting growth behavior was observed at 130 °C–250 °C, and the film growth rate was 1.4 Å/cycle. The GaN films deposited on the Si(100) substrate were crystalline with an atomic Ga/N ratio of 0.97, and the carbon and oxygen impurity concentrations were 2.8 at% and 3 at%, respectively.

Metal silylamides have also been used for ALD to deposit various materials, such as Li_3N [263], La_2O_3 [264], ZrO_2 [265], and PbI_2 [266]. The metal silylamides are highly reactive but not quite thermally stable, and the decomposition of the metal silylamides would leave silicon impurities in the films. For instance, in the ALD ZrO_2 films deposited from $ZrCl_2[N(SiMe_3)_2]_2$ and H_2O, the silicon concentration was found to be 1.1–5.4 at% for the deposition temperatures of 150 °C–350 °C [265]. On the other hand, silicon-containing W_xSi_yN thin films could be deposited from $W(N^tBu)_2[N(SiMe_3)_2]_2$ and H_2 plasma (figure 8(c)) [259].

3.7. Metal amidinates

Metal amidinates have been widely used as the ALD precursors. The amidinate ligands can bidentately coordinate to the metal ions to form chelated four-member ring structures. The chelation can considerably enhance the thermal stability, and therefore, the metal amidinates are generally more thermal stable than the metal amides. The chelation of the amidinates resembles that of the β-diketonates, but the nitrogen–metal coordination bonds are much weaker than the oxygen–metal bonds in β-diketonates, and therefore, the metal amidinates are usually of better reactivity. The amidinate side chains and backbones can be further substituted to modulate the volatility and reactivity of the complexes. Particularly for large-size metals, introducing bulky side alkyl chains is important to prevent oligomerization.

Metal amidinates have been used for the ALD of transition metals [73, 267], oxides [181–184], sulfides [86], and selenides [268]. For instance, Cu, Co, Fe, and Ni metals can be deposited from their *N,N′*-dialkylacetamidinate compounds together with the use of H_2 as the co-reactant [73]. As another example, cobalt oxides can be deposited from $Co(^iPr_2AMD)_2$ by using H_2O or O_3 as the co-reactant [267]. As shown in figure 9(a), using H_2O, rock-salt CoO films could be deposited at 150 °C–200 °C with a growth rate of 0.45 Å/cycle;

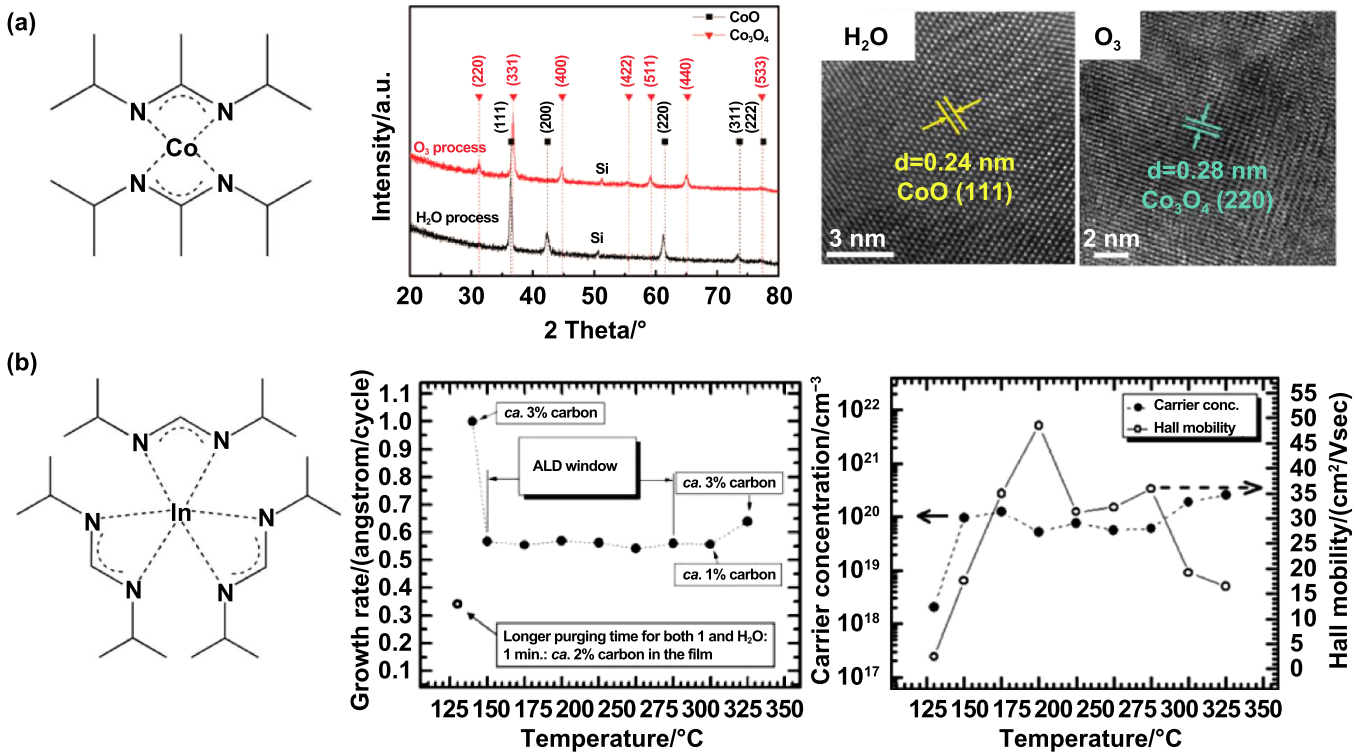

Figure 9. ALD from metal amidinates. (a) ALD of CoO_x from $Co(^iPr_2AMD)_2$ with the co-reactant of H_2O or O_3 [267]. John Wiley & Sons. © 2022 Wiley-VCH GmbH. (b) ALD of In_2O_3 from $In(^iPr_2FMD)_3$ and H_2O [187]. John Wiley & Sons. © 2018 Wiley-VCH Verlag GmbH & Co. KGaA, Weinheim.

whereas using O_3, spinel Co_3O_4 films could be deposited at 200 °C–225 °C with a growth rate of 0.5 Å/cycle. As for the metal sulfides, $M(^tBu_2AMD)_2$ (M = Fe, Co, Ni) could be used with molecular H_2S to deposit FeS_x [269], Co_9S_8 [185], and NiS_x [103], and they could also be used with H_2S plasma to deposit the metal disulfides of FeS_2, CoS_2, and NiS_2 [86]. Recently, these compounds were also used with diethyldiselenide (DEDSe) and Ar/H_2 plasma to deposit the metal selenides of $FeSe_2$, $CoSe_2$, and $NiSe_2$ [268].

Metal amidinates have also been used as the precursors for varieties of lanthanides and basic metals. $La(^iPr_2FMD)_3$ is a typical example. This compound is fairly volatile and has been extensively used for the ALD of the lanthanum-based oxides [193, 270, 271]. As for the basic metals, $In(^iPr_2FMD)_3$ [187] and $Sn(^iPr_2AMD)_2$ [260] have been reported as the precursors. For instance, $In(^iPr_2FMD)_3$ could be used with H_2O to deposit high-purity In_2O_3, and the film growth rate was 0.55 Å/cycle at 150 °C–275 °C (figure 9(b)) [187].

3.8. Heteroleptic metal precursors

Heteroleptic metal precursors are rapidly emerging in recent years. Two or more different ligands are bonded to the center metal atom in heteroleptic metal precursors, and a combination of the best properties of the respective parent homoleptic compounds can possibly be obtained [272]. For instance, the thermal stability of the metal precursors may be improved by incorporating the halide ligands; $ZrCp_2Cl_2$ [195] and $HfCp_2Cl_2$ [196] are thermally stable, without losing the self-limiting growth nature even at 300 and 350 °C, respectively. Cyclopentadienyl-alkylamido compounds have also been synthesized for zirconium [273], hafnium [274] and titanium [197]. Compared to their homoleptic metal amides, better thermal stability was obtained and the reactivity was comparable when using O_3 as co-reactant to deposit the oxide films. A recent study suggested that the cyclopentadienyl-alkylamido compounds chemisorbed to the film surfaces mainly through the reactions of the alkylamide ligands, and therefore, H_2O was difficult to be used as the co-reactant to deposit the oxide films [197].

The asymmetry of the heteroleptic compounds also helps the precursors to remain in liquid form. For instance, $M(^iPrCp)_2(^iPr_2AMD)$ (M = Y, La, Pr, Gd, and Dy) have been used to deposit the rare-earth oxide films [198, 199]. All these precursors are liquid and highly volatile. Using H_2O as the co-reactant, the oxide films could be deposited at no higher than 200 °C. It is worth noting that the hygroscopicity of the lanthanide oxides may lead to the loss of the self-limiting growth, and this problem can be solved by introducing O_3 as the oxygen source [199].

Notably, in some cases, the heteroleptic metal precursors do not exhibit improved properties, or even worse, some undesired properties of the respective homoleptic precursors may be introduced. Generally, the understanding about the chemistry of the heteroleptic compounds is still very limited, and the surface chemistry investigation is much needed.

3.9. ALD precursors for non-metals

Aside from the metal precursors, the precursors for the non-metal elements are also important for ALD. For instance, to deposit metal oxides, a variety of oxygen sources can be chosen. If the metal precursors are sufficiently reactive, H_2O is the most common oxygen source, and alcohols can sometimes be used. However, if the reactivity of the metal precursors is low, a strong oxidant, such as H_2O_2, O_2, O_3, or O_2 plasma, is usually needed. Notably, H_2O_2 and O_3 are prone to decompose at high temperature, and the deposited films may also catalyze this process [152], which would deteriorate the uniformity and conformality of the deposited films. As for the O_2 plasma, the O radicals in the plasma are reactive species, but the radicals are prone to recombine at the substrate surface and therefore possibly difficult to reach the bottom of a very deep trench. Therefore, conformal coating on high-aspect-ratio trenches may not be easy to realize. The O_2 plasma also contains oxygen ions, of which the motion can be anisotropic and therefore affect the deposition conformality [89].

The nitrogen precursors for the ALD of metal nitrides include NH_3 [212, 275], hydrazine [276], N_2 plasma [277, 278], and NH_3 plasma [261, 262]. NH_3 is commonly used, given that the metal precursors are sufficiently reactive [212, 275]. Some ALD processes use hydrazine [276], which is more reactive than NH_3, but this compound is toxic and explosive. N_2 or NH_3 plasma can be used to enhance the surface chemistry reactivity [262, 278]. In some cases, particularly for the deposition of low-resistivity metallic TiN and TaN_x, H_2 plasma or mixed H_2:N_2 plasma can be used to reduce the carbon impurity level in the deposited films [201, 278, 279].

As for chalcogenides, H_2S and H_2S plasma are often used to deposit the metal sulfides, despite that the H_2S gas is toxic and explosive. Recently, an organosulfur precursor of di-tert-butyl disulfide (TBDS) was reported to replace H_2S for the sulfide ALD [280]. Also, the alkylsilyl compounds of $(Et_3Si)_2Se$ and $(Et_3Si)_2Te$ are often used for the ALD of metal selenides and tellurides, respectively [134].

As for pnictogenides, PH_3 and AsH_3 have been used to deposit the metal phosphides [213] and arsenides [214], respectively. As for fluorides, HF is extremely toxic and corrosive, and therefore, alternatives, such as TiF_4 and TaF_5, have been used to deposit the metal fluorides [254].

4. Applications

ALD has already been extensively used in microelectronics industry, since the adoption of the high-k ZrO_2 in DRAM and subsequently the HfO_2 gate-dielectric in the Si-based 45 nm CMOS technology. As the microelectronics technology continues to advance, many new types of device structures have emerged and would need ALD to fabricate their essential components. To this end, we herein review a few newly-emerged areas in microelectronics, where ALD has considerably promising applications, including oxide-based transistors, ferroelectric dielectrics, and metal interconnects. It is worth noting that, other than microelectronics, ALD have also been used in many other areas, such as solar cells [281–284], supercapacitors [285–287], and catalysis [288–290], and the readers can find the reviews in the above-cited references.

4.1. Oxide-based transistors

With the fast development of artificial intelligence, the demand for computing power has increased significantly. In the past decades, the critical size of the transistors has been continually shrinking to boost the performance of the ICs. However, as the traditional Si-based transistor approaches its limitation of the critical size downscaling, new materials are needed to be introduced to the Si technology to further improve the ICs. The desired materials should have good immunity to short-channel effect, high mobility, and low contact resistance to achieve high-performance transistors. More importantly, the fabrication of the materials should have good compatibility with the BEOL process and the advanced device structures, such as FinFET and GAAFET. Oxide semiconductors, such as In_2O_3 [291–293], InGaO (IGO) [294–296], InZnSnO (IZTO) [297], and InGaZnO (IGZO) [14, 298, 299], have outstood as the promising materials for the new transistor and IC technology. The FETs made of oxide semiconductors have extremely low off-current and a reasonably high electron mobility (>10 cm^2 V^{-1} s^{-1}). More importantly, the fabrication of these oxide-based transistors needs fairly thermal budge, which is compatible with the BEOL requirement ($\leqslant$400 °C), and therefore, the oxide-based transistors are possible to be built directly on the traditional Si-based CMOS circuits to achieve 3D circuit integration. The ALD technique has been considered as a pivotal approach to fabricate these oxide-based transistors for its low process temperature and precise control of the film thickness and composition. With careful engineering of the involved surface chemistry and precursor chemistry, high-performance oxide transistors can be achieved by ALD. For instance, Si *et al* [291] demonstrated that using the ultrathin In_2O_3 (0.50 nm) channel layers made by ALD, the FETs with the channel length of 8.0 nm were able to achieve a very high on/off ratio of 10^{10} (figure 10(a)). Also, Cho *et al* [299] showed that the transistors using the amorphous IGZO (a-IGZO) channel layers made by ALD could achieve a high electron mobility of 36.6 cm^2 V^{-1} s^{-1} and a good bias stress stability.

Aside from the channel layer, the gate-dielectrics can also be made by ALD, and the afforded dielectric–channel interface can be achieved with very low trap density. For instance, Li *et al* [300] used ALD to deposit 4 nm Al_2O_3 as the gate-dielectric for the a-IGZO transistors, and owing to the good quality of the Al_2O_3/a-IGZO dielectric–channel interface, the afforded transistors showed a fairly low subthreshold swing of only 60.9 mV dec^{-1} and a very good bias stress stability (figure 10(b)). Cho *et al* [298] also reported high-performance transistors based on the ALD-prepared IGZO channel and stacked HfO_2–Al_2O_3 gate-dielectric, and the transistors exhibited a high electron mobility of 74.0 cm^2 V^{-1} s^{-1} with negligible hysteresis (figure 10(c)).

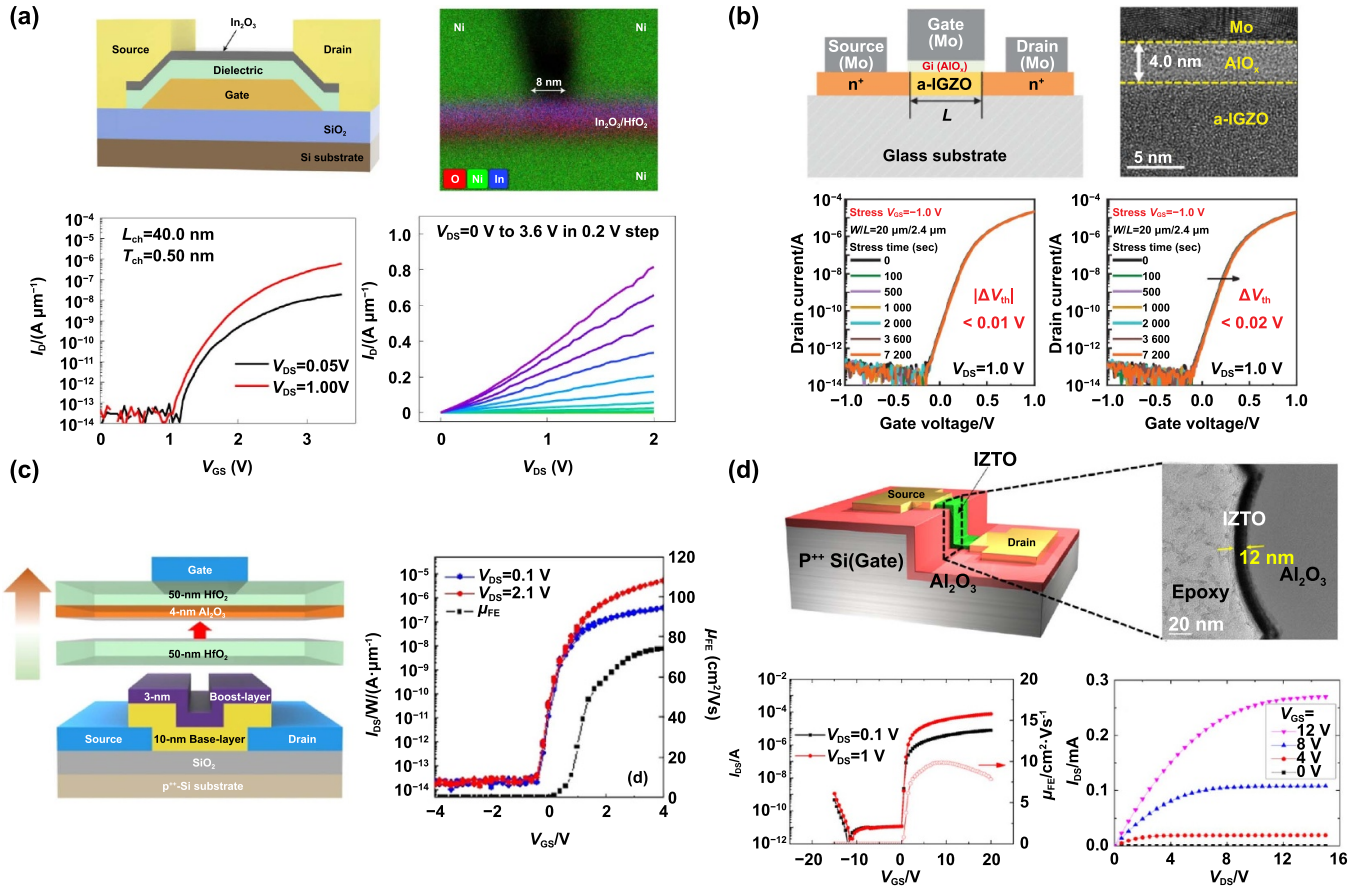

Figure 10. Oxide-based transistors fabricated by ALD. (a) ALD of the In_2O_3 channel layer for short-channel transistors: schematic structure, EDX elemental mapping, transfer and output characteristics. Reprinted by permission from Springer Nature Customer Service Centre GmbH: Nature, Nature Electronics [291], Copyright (2022). (b) Self-aligned top-gate a-IGZO transistors with a 4 nm Al_2O_3 gate-dielectric layer prepared by ALD: schematic structure, cross-sectional HRTEM image, and transfer characteristics under bias stress tests. © [2022] IEEE. Reprinted, with permission, from [300]. (c) Transistors with an ALD-prepared IGZO channel and stacked HfO_2–Al_2O_3 gate-dielectric: schematic illustration of the interface optimization, transfer characteristics, and field-effect mobility. Reprinted with permission from [298]. Copyright (2021) American Chemical Society. (d) Vertical transistors based on ALD IZTO and Al_2O_3: schematic structure, cross-sectional TEM image, transfer and output characteristics. Reprinted with permission from [297]. Copyright (2019) American Chemical Society.

As a step forward, both the oxide channel and gate-dielectric layers can be made by ALD. With the unique feature of ALD for conformal coating, both the layers can be deposited on vertical side walls or in hole structures to realize vertical-structure transistors. For instance, Baek *et al* [297] showed that vertical oxide transistors could be fabricated on side walls based on the ALD-prepared IZTO channel layer and Al_2O_3 dielectric layer (figure 10(d)). Also, Chen *et al* [15] demonstrated that vertical channel-all-around (CAA) FETs could be fabricated in hole structures by ALD. Compared to the traditional planar FETs, the vertical CAA FETs have a much smaller lateral size, which can be utilized to fabricate high-density 2T0C DRAM with $4F^2$ cell structure. All these results have shown the great promise of ALD to prepare high-performance oxide-based transistors.

4.2. Ferroelectric dielectrics

As the traditional transistor reach its physical limitation, the novel computing architectures, such as in-memory computing, are also attractive to boost the performance of the ICs beyond the Moore's law. Ferroelectricity is featured for the presence of two states of spontaneous electric polarization that can be reversibly switched by an applied electric field. The two-state behavior can be utilized for the binary data processing in digital computing, which perfectly meets the requirements of the in-memory computing. The HfO_2-based ferroelectric materials can be deposited by ALD, which is well compatible with the contemporary IC fabrication, and therefore, the HfO_2-based materials are highly promising for building new devices based on the ferroelectricity [301]. The ferroelectricity of the ultrathin HfZrO (HZO) films deposited by ALD was confirmed by Cheema *et al* [302]. The composition of the HZO films could be tuned by the subcycle numbers for HfO_2 and ZrO_2, and switchable polarization was observable even for the HZO thickness downscaling to 1 nm (figure 11(a)).

The HfO_2-based ferroelectric materials are well suited for non-volatile memories for their low power consumption to switch the polarity. This new type of memories has a higher density than the traditional DRAM. Luo *et al* [303] fabricated

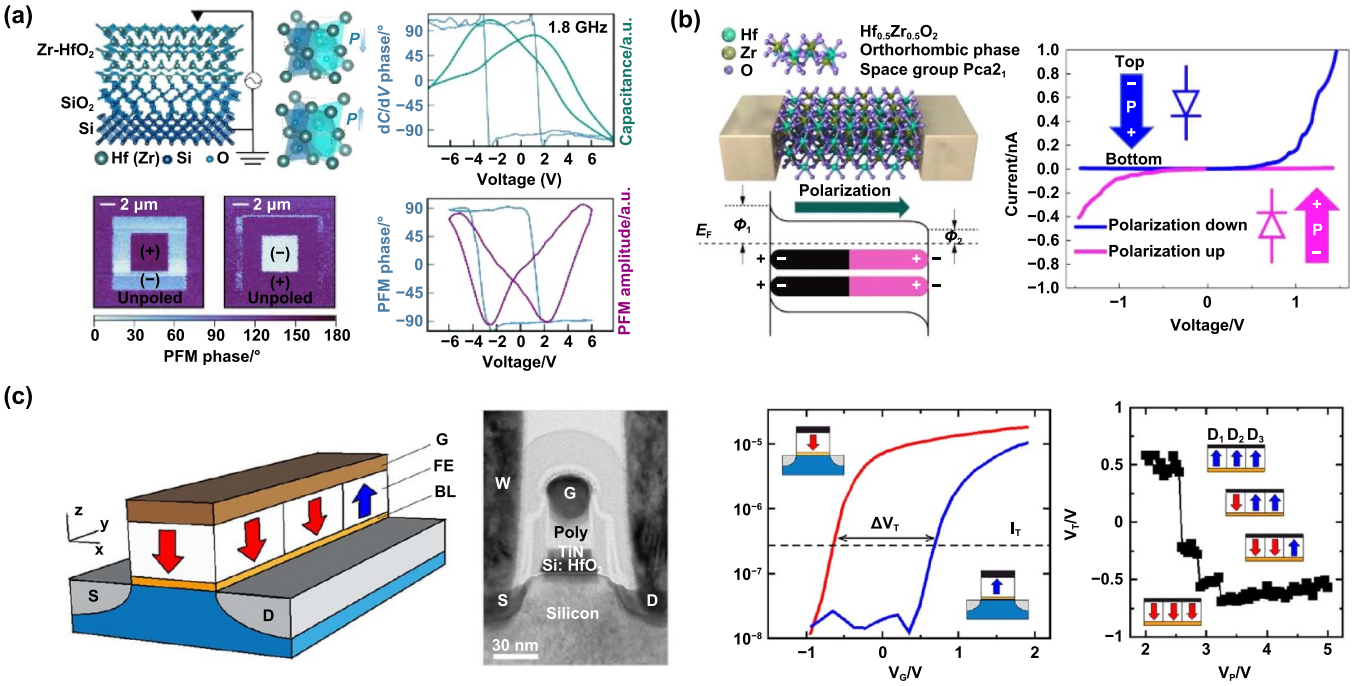

Figure 11. ALD prepared ferroelectric dielectrics. (a) Ultrathin ferroelectric HZO films deposited by ALD: schematic HZO unit cell, C–V characteristics, phase-contrast PFM image, and PFM hysteresis loops. Reprinted by permission from Springer Nature Customer Service Centre GmbH: Nature [302], Copyright (2020). (b) Ferroelectric diodes based on ALD HZO: schematic structure, energy band diagrams, and nonlinear diode-like I–V characteristics. Reprinted by permission from Springer Nature Customer Service Centre GmbH: Nature, Nature Communications [303], Copyright (2020). (c) Ferroelectric FETs based on ALD Si:HfO_2: schematic structure, cross-sectional TEM image, hysteresis of transfer characteristics, and threshold voltage (V_T) versus the programing voltage (V_P). Reprinted with permission from [304]. Copyright (2017) American Chemical Society.

the ferroelectric HZO diodes by ALD and implemented these diodes in an eight-layer 3D array for memory applications. The diode memory devices showed a high operation speed of 20 ns and robust endurance of $>10^9$ (figure 11(b)). Another attractive application is the ferroelectric FETs, in which the transistor threshold voltage can be controlled by the polarization state of the ferroelectric layer. For instance, Halid *et al* [304] showed that the ALD Si:HfO_2 could be implemented to fabricate ultrascaled ferroelectric FETs, and domain-level ferroelectric switching could be directly observed (figure 11(c)). Liao *et al* [305] demonstrated that 3D GAA nanosheet ferroelectric FETs could be made based on the ALD HZO, and the devices showed a large memory window of 1.3 V, robust endurance cycles of $>10^{11}$, and stable data retention of $>20\,000$ s. All these results indicate that, with the ALD technology, the dimensional scaling of the ferroelectric devices is highly promising for future advanced memory and computing technologies.

4.3. Metal interconnects

As the technology node of integrated ICs continues to shrink down to 3 nm and beyond, the increasing density of the transistors has led to a significant increase in the interconnect complexity, and this complexity presents serious challenges to the BEOL interconnect fabrication. In particular, the linewidths of the local interconnects in the first few interconnect layers are less than 20 nm and their aspect ratios are more than 4:1. Hence, it is necessary to achieve uniform sub-nm thicknesses for the barrier/liner/seed layers in trenches and vias to ensure enough space for electroplating the metal wires. This is obviously a great challenge for the traditional PVD because of its tendency to form overhangs, as shown in figure 12(a) [306]. Severe overhangs leave only a small gap space to fill the metal, which would result in the increase of the line resistance and resistance–capacitance delay, and also reduce the interconnect reliability. ALD has the advantages of high uniformity, excellent step coverage, and atomic-scale thickness control, which makes it one of the key technologies for advanced interconnect fabrication, as shown in figure 12(a). To be compatible with the process temperature limit of BEOL ($\leqslant$400 °C), the thin-film coatings can be prepared by PALD. In the damascene Cu process, TaN, Ta, and Cu metals are used as the barrier, liner, and seed layers, respectively [307]. All these metals can be prepared by PALD. For instant, low-resistivity TaN films can be deposited from tertbutylimidotris(diethylamido)tantalum (TBTDET) and H_2 plasma [308]. The Ta films can be deposited from $TaCl_5$ and H_2 plasma [128, 309]. The high-quality Cu seed layers can be deposited from $Cu(acac)_2$ for interconnects [310]. In another case, Guo *et al* reported that the Cu thin films could be deposited from $[Cu(^iPr_2AMD)]_2$ and H_2 plasma at temperature as low as 50 °C, and the

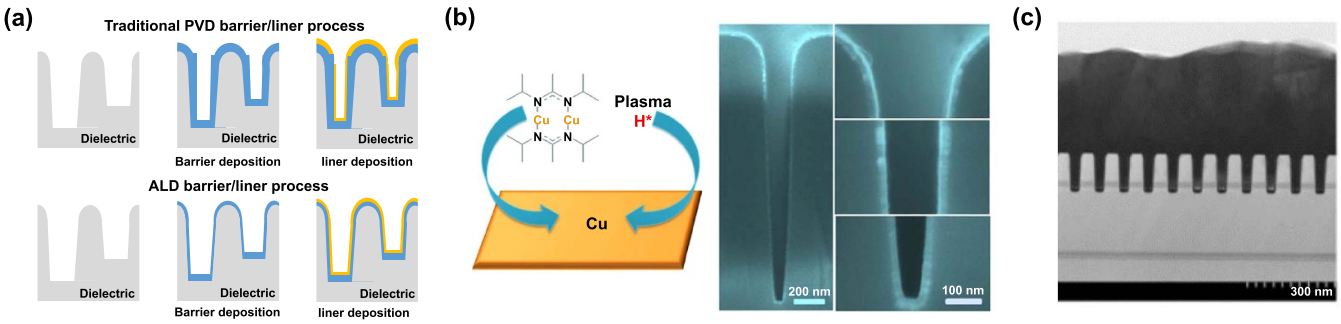

Figure 12. ALD for metal interconnects. (a) Schematic illustration of the PVD and ALD barrier/liner processes. (b) ALD of Cu films from $[Cu(^{i}Pr_2AMD)]_2$ and H_2 plasma inside a 10:1 trench. Reprinted with permission from [186]. Copyright (2015) American Chemical Society. (c) ALD of Co films inside 24 nm-deep trenches for direct Cu electroplating. Reprinted from [311], Copyright (2014), with permission from Elsevier.

properties of the ALD Cu films, such as continuity, uniformity, and resistivity, were comparable to the PVD Cu films (figure 12(b)) [186].

As the Cu interconnect technology advances, Co and Ru have been developed to replace Ta as the liner material. Co and Ru have a better wettability with Cu, which can facilitate the filling of Cu during the electroplating, and they can also improve the overall integrity of the TaN barrier [312, 313]. For example, Park *et al* demonstrated that the Co films deposited from dicobalt hexacarbonyl tert-butylacetylene (CCTBA) and H_2 plasma could be used for direct Cu electroplating (figure 12(c)) [311]. Swerts *et al* reported that the Ru films could be deposited from (MeCpPy)Ru and N_2/NH_3 plasma at 330 °C for interconnect applications [314]. In the advanced interconnect technology, Cu wires have been gradually replaced by Co or Ru for high-conductivity narrow interconnects [315]. The Co interconnects have been used in the advanced nodes of chip fabrication, while the Ru interconnects are still at the laboratory research stage. The barrier and liner materials of these two interconnects are TiN and Ti, respectively, which can also be obtained by PALD [128, 316]. Therefore, ALD is a critical fabrication technology for the advanced IC interconnects.

5. Summary and outlook

In summary, ALD is a unique technology to deposit highly uniform conformal thin films with atomic-level controllability, and it has become extensively applied to varieties of applications along with decades of development. To achieve the precise control over the film thickness, morphology, conformality, and composition, understanding the involved self-limiting surface chemical reactions is crucial. The surface chemistry mechanisms can be generally classified into four categories, which are the ligand-exchange, dissociative or non-dissociative chemisorption, oxidation, and reduction mechanisms. These mechanisms are not fully separate, and in many cases, an ALD process might consist of multiple reaction mechanisms. Nonideal factors, such as nucleation delay, byproduct adsorption, ligand decomposition, agglomeration, and ion diffusion can also be present in some ALD processes, and these nonideal factors can greatly influence the morphology and impurity of the deposited films. The precursor chemistry is also very important. To this end, we elaborately discussed various types of the compounds that have been used as the ALD precursors. Particularly, for the metalorganic precursors, the design of the ligand structures is the key to achieve the desired features of high volatility, high thermal stability, and good self-limiting reactivity. Then, we discussed a few emerging applications of the ALD technology for microelectronics, including BEOL-compatible oxide-based transistors, ferroelectric dielectrics, and metal interconnects. All these applications indicate an increasingly important role of ALD for future advanced IC technologies.

Over the past decades, the ALD technology has been developing very rapidly; however, many challenges remain to be solved. For instance, there are still many materials that have not been synthesized by ALD. Particularly, the multielement compounds (e.g. ternary and quaternary compounds) are challenging to tune their elemental composition continuously by ALD [22]. Currently, the common approach to deposit the multicomponent compounds is to use the supercycles that consist of the ALD subcycles for the constituent binary compounds. In this approach, the tuning of the composition is discrete, and moreover, the afforded composition is often deviated from the expectation that is based on the ALD growth rates of the individual binaries. This deviation is mainly because, in the supercycle manner, the nucleation effects are substantially amplified, owing to the frequently switching between the depositions of different materials. To tackle this issue, surface chemistry investigation and precursor engineering is much needed to elucidate and tune the nucleation behavior.

On the separate note, area-selective ALD is an emerging technology that has recently attracted increasing attention. This technology is of great potential for the applications in the microelectronics industry to eliminate the edge placement errors in photolithography [12]. To realize this technology reliable for the industrial applications, it is necessary to

understand the relevant surface chemistry so as to accordingly design the ALD precursors that can grow only on the target areas.

In addition, the throughput is often a limiting factor of ALD for high-volume manufacturing. The batch-type ALD systems are capable of processing thousands of wafers simultaneously, and they have been used in the manufacturing of solar cells [317]. Spatial ALD has also been considered as a solution to improve the throughput [317–319]. In spatial ALD, the surface chemical reactions are separated in space, rather than in time as in the conventional ALD. However, the spatial ALD approach is more sensitive to the kinetics of the surface chemical reactions, and therefore, the surface chemistry and precursor chemistry is even more important for this technology toward large-scale manufacturing.

In conclusion, chemistry plays a decisive role in the ALD technology. A comprehensive understanding of the ALD chemistry can significantly promote the development and application of the ALD technology.

Acknowledgments

This work was supported by NSFC (22175005), Guangdong Basic and Applied Basic Research Foundation (2020B 1515120039), Shenzhen Fundamental Research Program (JCYJ20200109110628172, GXWD20201231165807007-20200802205241003), and Guangdong Technology Center for Oxide Semiconductor Devices and ICs.

ORCID iDs

Jinxiong Li https://orcid.org/0000-0001-5284-9020
Gaoda Chai https://orcid.org/0000-0002-0887-3290
Xinwei Wang https://orcid.org/0000-0002-1191-8162

References

[1] Salahuddin S, Ni K and Datta S 2018 The era of hyper-scaling in electronics *Nat. Electron.* **1** 442–50
[2] Hisamoto D, Lee W C, Kedzierski J, Takeuchi H, Asano K, Kuo C, Anderson E, King T J, Bokor J and Hu C M 2000 FinFET—a self-aligned double-gate MOSFET scalable to 20 nm *IEEE Trans. Electron Devices* **47** 2320–5
[3] Singh N *et al* 2006 High-performance fully depleted silicon nanowire (diameter $\leqslant$ 5 nm) gate-all-around CMOS devices *IEEE Electron. Device Lett.* **27** 383–6
[4] George S M 2010 Atomic layer deposition: an overview *Chem. Rev.* **110** 111–31
[5] Puurunen R L 2005 Surface chemistry of atomic layer deposition: a case study for the trimethylaluminum/water process *J. Appl. Phys.* **97** 121301
[6] Richey N E, De Paula C and Bent S F 2020 Understanding chemical and physical mechanisms in atomic layer deposition *J. Chem. Phys.* **152** 040902
[7] Mei C Y, Shen W C, Wu C H, Chih Y D, King Y C, Lin C J, Tsai M J, Tsai K H and Chen F T 2013 28-nm 2T high-*K* metal gate embedded RRAM with fully compatible CMOS logic processes *IEEE Electron Device Lett.* **34** 1253–5
[8] Cai M, Ramani K, Belyansky M, Greene B, Lee D H, Waidmann S, Tamweber F and Henson W 2010 Stress liner effects for 32-nm SOI MOSFETs with HKMG *IEEE Trans. Electron Devices* **57** 1706–9
[9] Pešić M *et al* 2016 Low leakage ZrO_2 based capacitors for sub 20 nm dynamic random access memory technology nodes *J. Appl. Phys.* **119** 064101
[10] Knebel S, Pesic M, Cho K, Chang J, Lim H, Kolomiiets N, Afanas'ev V V, Muehle U, Schroeder U and Mikolajick T 2015 Ultra-thin ZrO_2/SrO/ZrO_2 insulating stacks for future dynamic random access memory capacitor applications *J. Appl. Phys.* **117** 224102
[11] Natarajan S *et al* 2014. A 14nm logic technology featuring 2nd-generation FinFET, air-gapped interconnects, self-aligned double patterning and a 0.0588 μm^2 SRAM cell size *2014 IEEE International Electron Devices Meeting* (San Francisco, CA: IEEE) pp 3.7.1–3
[12] Clark R, Tapily K, Yu K H, Hakamata T, Consiglio S, O'Meara D, Wajda C, Smith J and Leusink G 2018 Perspective: new process technologies required for future devices and scaling *APL Mater.* **6** 058203
[13] Sheng J Z, Lee J H, Choi W H, Hong T, Kim M and Park J S 2018 Review article: atomic layer deposition for oxide semiconductor thin film transistors: advances in research and development *J. Vac. Sci. Technol.* A **36** 060801
[14] Sheng J Z, Hong T, Lee H M, Kim K, Sasase M, Kim J, Hosono H and Park J S 2019 Amorphous IGZO TFT with high mobility of $\sim$70 cm^2/(V s) via vertical dimension control using PEALD *ACS Appl. Mater. Interfaces* **11** 40300–9
[15] Chen Q *et al* 2022 Investigation of asymmetric characteristics of novel vertical channel-all-around (CAA) In-Ga-Zn-O field effect transistors *IEEE Electron Device Lett.* **43** 894–7
[16] Wang X W 2021 Atomic layer deposition of iron, cobalt, and nickel chalcogenides: progress and outlook *Chem. Mater.* **33** 6251–68
[17] Profijt H B, Potts S E, Van De Sanden M C M and Kessels W M M 2011 Plasma-assisted atomic layer deposition: basics, opportunities, and challenges *J. Vac. Sci. Technol.* A **29** 050801
[18] Lee Y *et al* 2021 Growth mechanism and electrical properties of tungsten films deposited by plasma-enhanced atomic layer deposition with chloride and metal organic precursors *Appl. Surf. Sci.* **568** 150939
[19] Miikkulainen V, Leskelä M, Ritala M and Puurunen R L 2013 Crystallinity of inorganic films grown by atomic layer deposition: overview and general trends *J. Appl. Phys.* **113** 021301
[20] Cremers V, Puurunen R L and Dendooven J 2019 Conformality in atomic layer deposition: current status overview of analysis and modelling *Appl. Phys. Rev.* **6** 021302
[21] Mackus A J M, Merkx M J M and Kessels W M M 2019 From the bottom-up: toward area-selective atomic layer deposition with high selectivity *Chem. Mater.* **31** 2–12
[22] Mackus A J M, Schneider J R, MacIsaac C, Baker J G and Bent S F 2019 Synthesis of doped, ternary, and quaternary materials by atomic layer deposition: a review *Chem. Mater.* **31** 1142–83
[23] Meng X B, Wang X W, Geng D S, Ozgit-Akgun C, Schneider N and Elam J W 2017 Atomic layer deposition for nanomaterial synthesis and functionalization in energy technology *Mater. Horiz.* **4** 133–54
[24] Cao K, Cai J M and Chen R 2020 Inherently selective atomic layer deposition and applications *Chem. Mater.* **32** 2195–207
[25] Hagen D J, Pemble M E and Karppinen M 2019 Atomic layer deposition of metals: precursors and film growth *Appl. Phys. Rev.* **6** 041309

[26] Hämäläinen J, Ritala M and Leskelä M 2014 Atomic layer deposition of noble metals and their oxides *Chem. Mater.* **26** 786–801

[27] Gordon P G, Kurek A and Barry S T 2015 Trends in copper precursor development for CVD and ALD applications *ECS J. Solid State Sci. Technol.* **4** N3188–97

[28] Knisley T J, Kalutarage L C and Winter C H 2013 Precursors and chemistry for the atomic layer deposition of metallic first row transition metal films *Coord. Chem. Rev.* **257** 3222–31

[29] Knapas K and Ritala M 2013 *In situ* studies on reaction mechanisms in atomic layer deposition *Crit. Rev. Solid State Mater. Sci.* **38** 167–202

[30] Barry S T, Gordon P G and Vandalon V 2022 Common precursors and surface mechanisms for atomic layer deposition *Comprehensive Organometallic Chemistry IV* vol 14 pp 534–52

[31] Muneshwar T, Barlage D and Cadien K 2021 Stoichiometry controlled homogeneous ternary oxide growth in showerhead atomic layer deposition reactor and application for $Zr_xHf_{1-x}O_2$ *J. Vac. Sci. Technol.* A **39** 030401

[32] Arroval T, Aarik L, Rammula R and Aarik J 2015 Growth of $Ti_xAl_{1-x}O_y$ films by atomic layer deposition using successive supply of metal precursors *Thin Solid Films* **591** 276–84

[33] Bielinski A R, Kamphaus E P, Cheng L and Martinson A B F 2022 Resolving the heat of trimethylaluminum and water atomic layer deposition half-reactions *J. Am. Chem. Soc.* **144** 15203–10

[34] Guerra-Nunez C, Dobeli M, Michler J and Utke I 2017 Reaction and growth mechanisms in Al_2O_3 deposited via atomic layer deposition: elucidating the hydrogen source *Chem. Mater.* **29** 8690–703

[35] Oh I K, Sandoval T E, Liu T L, Richey N E, Nguyen C T, Gu B, Lee H B R, Tonner-Zech R and Bent S F 2022 Elucidating the reaction mechanism of atomic layer deposition of Al_2O_3 with a series of $Al(CH_3)_xCl_{3-x}$ and $Al(C_yH_{2y+1})_3$ precursors *J. Am. Chem. Soc.* **144** 11757–66

[36] Seghete D, Rayner G B Jr, Cavanagh A S, Anderson V R and George S M 2011 Molybdenum atomic layer deposition using MoF_6 and Si_2H_6 as the reactants *Chem. Mater.* **23** 1668–78

[37] Sechrist Z A, Fabreguette F H, Heintz O, Phung T M, Johnson D C and George S M 2005 Optimization and structural characterization of W/Al_2O_3 nanolaminates grown using atomic layer deposition techniques *Chem. Mater.* **17** 3475–85

[38] Grubbs R K, Steinmetz N J and George S M 2004 Gas phase reaction products during tungsten atomic layer deposition using WF_6 and Si_2H_6 *J. Vac. Sci. Technol.* B **22** 1811–21

[39] Zanders D, Liu J, Obenlüneschloß J, Bock C, Rogalla D, Mai L, Nolan M, Barry S T and Devi A 2021 Cobalt metal ALD: understanding the mechanism and role of zinc alkyl precursors as reductants for low-resistivity co thin films *Chem. Mater.* **33** 5045–57

[40] Lee B H, Hwang J K, Nam J W, Lee S U, Kim J T, Koo S M, Baunemann A, Fischer R A and Sung M M 2009 Low-temperature atomic layer deposition of copper metal thin films: self-limiting surface reaction of copper dimethylamino-2-propoxide with diethylzinc *Angew. Chem., Int. Ed.* **48** 4536–9

[41] Lu J L and Elam J W 2015 Low temperature ABC-type Ru atomic layer deposition through consecutive dissociative chemisorption, combustion, and reduction steps *Chem. Mater.* **27** 4950–6

[42] Qin X D and Zaera F 2018 Chemistry of ruthenium diketonate atomic layer deposition (ALD) precursors on metal surfaces *J. Phys. Chem.* C **122** 13481–91

[43] Ma Q, Guo H S, Gordon R G and Zaera F 2010 Uptake of copper acetamidinate ALD precursors on nickel surfaces *Chem. Mater.* **22** 352–9

[44] Ma Q, Guo H S, Gordon R G and Zaera F 2011 Surface chemistry of copper(I) acetamidinates in connection with atomic layer deposition (ALD) processes *Chem. Mater.* **23** 3325–34

[45] Elko-Hansen T D M and Ekerdt J G 2014 XPS investigation of the atomic layer deposition half reactions of bis(N-*tert*-butyl-N′-ethylpropionamidinato) cobalt(II) *Chem. Mater.* **26** 2642–6

[46] Puurunen R L 2005 Correlation between the growth-per-cycle and the surface hydroxyl group concentration in the atomic layer deposition of aluminum oxide from trimethylaluminum and water *Appl. Surf. Sci.* **245** 6–10

[47] Elliott S D and Greer J C 2004 Simulating the atomic layer deposition of alumina from first principles *J. Mater. Chem.* **14** 3246–50

[48] Hämäläinen J, Hatanpää T, Puukilainen E, Sajavaara T, Ritala M and Leskelä M 2011 Iridium metal and iridium oxide thin films grown by atomic layer deposition at low temperatures *J. Mater. Chem.* **21** 16488–93

[49] Leick N, Verkuijlen R O F, Lamagna L, Langereis E, Rushworth S, Roozeboom F, Van De Sanden M C M and Kessels W M M 2011 Atomic layer deposition of Ru from $CpRu(CO)_2Et$ using O_2 gas and O_2 plasma *J. Vac. Sci. Technol.* A **29** 021016

[50] Kwon D S, An C H, Kim S H, Kim D G, Lim J, Jeon W and Hwang C S 2020 Atomic layer deposition of Ru thin films using (2,4-dimethyloxopentadienyl) (ethylcyclopentadienyl)Ru and the effect of ammonia treatment during the deposition *J. Mater. Chem.* C **8** 6993–7004

[51] Knapas K and Ritala M 2011 *In situ* reaction mechanism studies on atomic layer deposition of Ir and IrO_2 from $Ir(acac)_3$ *Chem. Mater.* **23** 2766–71

[52] Hwang J M *et al* 2021 Atomic layer deposition of a ruthenium thin film using a precursor with enhanced reactivity *J. Mater. Chem.* C **9** 3820–5

[53] Hämäläinen J, Sajavaara T, Puukilainen E, Ritala M and Leskelä M 2012 Atomic layer deposition of osmium *Chem. Mater.* **24** 55–60

[54] Aaltonen T, Ritala M and Leskela M 2005 ALD of rhodium thin films from $Rh(acac)_3$ and oxygen *Electrochem. Solid-State Lett.* **8** C99–C101

[55] Zou Y M, Cheng C Y, Guo Y Y, Ong A J, Goei R, Li S Z and Tok A I Y 2021 Atomic layer deposition of rhodium and palladium thin film using low-concentration ozone *RSC Adv.* **11** 22773–9

[56] Comstock D J, Christensen S T, Elam J W, Pellin M J and Hersam M C 2010 Tuning the composition and nanostructure of Pt/Ir films via anodized aluminum oxide templated atomic layer deposition *Adv. Funct. Mater.* **20** 3099–105

[57] Park N Y *et al* 2022 Atomic layer deposition of iridium using a tricarbonyl cyclopropenyl precursor and oxygen *Chem. Mater.* **34** 1533–43

[58] Molenbroek A M, Haukka S and Clausen B S 1998 Alloying in Cu/Pd nanoparticle catalysts *J. Phys. Chem.* B **102** 10680–9

[59] Zou Y M, Li J H, Cheng C Y, Wang Z W, Ong A J, Goei R, Li X L, Li S Z and Tok A I Y 2021 Atomic layer deposition of palladium thin film from palladium (II) hexafluoroacetylacetonate and ozone reactant *Thin Solid Films* **738** 138955

[60] Kim M, Nabeya S, Han S M, Kim M, Lee S, Kim H M, Cho S Y, Lee D J, Kim S H and Kim K B 2020 Selective atomic layer deposition of metals on graphene for

transparent conducting electrode application *ACS Appl. Mater. Interfaces* **12** 14331–40
[61] Dendooven J *et al* 2020 Surface mobility and impact of precursor dosing during atomic layer deposition of platinum: *in situ* monitoring of nucleation and island growth *Phys. Chem. Chem. Phys.* **22** 24917–33
[62] Liu P F, Zhang Y C, Liu C, Emery J D, Das A, Bedzyk M J, Hock A S and Martinson A B F 2021 Thermal atomic layer deposition of gold: mechanistic insights, nucleation, and epitaxy *ACS Appl. Mater. Interfaces* **13** 9091–100
[63] Mäkelä M, Hatanpää T, Mizohata K, Räisänen J, Ritala M and Leskelä M 2017 Thermal atomic layer deposition of continuous and highly conducting gold thin films *Chem. Mater.* **29** 6130–6
[64] Wu Y Z, Macco B, Vanhemel D, Kölling S, Verheijen M A, Koenraad P M, Kessels W M M and Roozeboom F 2017 Atomic layer deposition of In_2O_3:H from InCp and H_2O/O_2: microstructure and isotope labeling studies *ACS Appl. Mater. Interfaces* **9** 592–601
[65] Heo J, Liu Y Q, Sinsermsuksakul P, Li Z F, Sun L Z, Noh W and Gordon R G 2011 (Sn,Al)O_x films grown by atomic layer deposition *J. Phys. Chem.* C **115** 10277–83
[66] Heo J, Hock A S and Gordon R G 2010 Low temperature atomic layer deposition of Tin oxide *Chem. Mater.* **22** 4964–73
[67] Dai M, Kwon J, Halls M D, Gordon R G and Chabal Y J 2010 Surface and interface processes during atomic layer deposition of copper on silicon oxide *Langmuir* **26** 3911–7
[68] Setthapun W *et al* 2010 Genesis and evolution of surface species during Pt atomic layer deposition on oxide supports characterized by *in situ* XAFS analysis and water-gas shift reaction *J. Phys. Chem.* C **114** 9758–71
[69] Ten Eyck G A, Pimanpang S, Bakhru H, Lu T M and Wang G C 2006 Atomic layer deposition of Pd on an oxidized metal substrate *Chem. Vap. Depos.* **12** 290–4
[70] Utriainen M, Kröger-Laukkanen M, Johansson L S and Niinistö L 2000 Studies of metallic thin film growth in an atomic layer epitaxy reactor using M(acac)$_2$ (M = Ni, Cu, Pt) precursors *Appl. Surf. Sci.* **157** 151–8
[71] Lee H B R, Kim W H, Lee J W, Kim J M, Heo K, Hwang I C, Park Y, Hong S and Kim H 2010 High quality area-selective atomic layer deposition co using ammonia gas as a reactant *J. Electrochem. Soc.* **157** D10–D15
[72] Lee S J and Kim S H 2016 Effects of annealing on the properties of atomic layer deposited Ru thin films deposited by NH_3 and H_2 as reactants *Thin Solid Films* **612** 122–7
[73] Lim B S, Rahtu A and Gordon R G 2003 Atomic layer deposition of transition metals *Nat. Mater.* **2** 749–54
[74] Kim W H, Lee H B R, Heo K, Lee Y K, Chung T M, Kim C G, Hong S, Heo J and Kim H 2011 Atomic layer deposition of Ni thin films and application to area-selective deposition *J. Electrochem. Soc.* **158** D1–D5
[75] Cwik S, Woods K N, Saly M J, Knisley T J and Winter C H 2020 Thermal atomic layer deposition of ruthenium metal thin films using nonoxidative coreactants *J. Vac. Sci. Technol.* A **38** 012402
[76] Sarr M, Bahlawane N, Arl D, Dossot M, McRae E and Lenoble D 2014 Tailoring the properties of atomic layer deposited nickel and nickel carbide thin films via chain-length control of the alcohol reducing agents *J. Phys. Chem.* C **118** 23385–92
[77] Huo J S, Solanki R and McAndrew J 2002 Characteristics of copper films produced via atomic layer deposition *J. Mater. Res.* **17** 2394–8
[78] Elam J W, Zinovev A, Han C Y, Wang H H, Welp U, Hryn J N and Pellin M J 2006 Atomic layer deposition of palladium films on Al_2O_3 surfaces *Thin Solid Films* **515** 1664–73
[79] Premkumar P A, Bahlawane N, Reiss G and Kohse-Höinghaus K 2007 CVD of metals using alcohols and metal acetylacetonates, Part II: role of solvent and characterization of metal films made by pulsed spray evaporation CVD *Chem. Vap. Depos.* **13** 227–31
[80] Bahlawane N, Premkumar P A, Brechling A, Reiss G and Kohse-Höinghaus K 2007 Alcohol-assisted CVD of silver using commercially available precursors *Chem. Vap. Depos.* **13** 401–7
[81] Tiznado H and Zaera F 2006 Surface chemistry in the atomic layer deposition of TiN films from $TiCl_4$ and ammonia *J. Phys. Chem.* B **110** 13491–8
[82] Bouman M and Zaera F 2011 Reductive eliminations from amido metal complexes: implications for metal film deposition *J. Electrochem. Soc.* **158** D524–6
[83] Fix R M, Gordon R G and Hoffman D M 1990 Synthesis of thin films by atmospheric pressure chemical vapor deposition using amido and imido titanium(IV) compounds as precursors *Chem. Mater.* **2** 235–41
[84] Kim S, Woo S, Kim H, Jeong W, Park T, Kim H, Kim S B and Jeon H 2007 Atomic layer deposited $HfO_2/HfSi_xO_yN_z$ stacked gate dielectrics for metal-oxide-semiconductor structures *J. Vac. Sci. Technol.* B **25** 1922–7
[85] Maeng W J and Kim H 2007 Atomic scale nitrogen depth profile control during plasma enhanced atomic layer deposition of high *k* dielectrics *Appl. Phys. Lett.* **91** 092901
[86] Guo Z and Wang X W 2018 Atomic layer deposition of the metal pyrites FeS_2, CoS_2, and NiS_2 *Angew. Chem., Int. Ed.* **57** 5898–902
[87] Sobell Z C and George S M 2022 Electron-enhanced atomic layer deposition of titanium nitride films using an ammonia reactive background gas *Chem. Mater.* **34** 9624–33
[88] Knoops H C M, Langereis E, Van De Sanden M C M and Kessels W M M 2012 Reaction mechanisms of atomic layer deposition of TaN_x from $Ta(NMe_2)_5$ precursor and H_2-based plasmas *J. Vac. Sci. Technol.* A **30** 01A101
[89] Arts K, Deijkers J H, Faraz T, Puurunen R L, Kessels W M M and Knoops H C M 2020 Evidence for low-energy ions influencing plasma-assisted atomic layer deposition of SiO_2: impact on the growth per cycle and wet etch rate *Appl. Phys. Lett.* **117** 031602
[90] Boris D R, Wheeler V D, Nepal N, Qadri S B, Walton S G and Eddy C R 2020 The role of plasma in plasma-enhanced atomic layer deposition of crystalline films *J. Vac. Sci. Technol.* A **38** 040801
[91] Profijt H B, Van De Sanden M C M and Kessels W M M 2012 Substrate biasing during plasma-assisted ALD for crystalline phase-control of TiO_2 thin films *Electrochem. Solid-State Lett.* **15** G1–G3
[92] Faraz T, Verstappen Y G P, Verheijen M A, Chittock N J, Lopez J E, Heijdra E, Van Gennip W J H, Kessels W M M and Mackus A J M 2020 Precise ion energy control with tailored waveform biasing for atomic scale processing *J. Appl. Phys.* **128** 213301
[93] Argile C and Rhead G E 1989 Adsorbed layer and thin film growth modes monitored by auger electron spectroscopy *Surf. Sci. Rep.* **10** 277–356
[94] Gusev E P, Cabral J C, Copel M, D'Emic C and Gribelyuk M 2003 Ultrathin HfO_2 films grown on silicon by atomic layer deposition for advanced gate dielectrics applications *Microelectron. Eng.* **69** 145–51
[95] Copel M, Gribelyuk M and Gusev E 2000 Structure and stability of ultrathin zirconium oxide layers on Si(001) *Appl. Phys. Lett.* **76** 436–8
[96] Aaltonen T, Alén P, Ritala M and Leskelä M 2003 Ruthenium thin films grown by atomic layer deposition *Chem. Vap. Depos.* **9** 45–49

[97] Oh I K, Park B E, Seo S, Yeo B C, Tanskanen J, Lee H B R, Kim W H and Kim H 2018 Comparative study of the growth characteristics and electrical properties of atomic-layer-deposited HfO_2 films obtained from metal halide and amide precursors *J. Mater. Chem.* C **6** 7367–76

[98] Park B E, Oh I K, Lee C W, Lee G, Shin Y H, Lansalot-Matras C, Noh W, Kim H and Lee H B R 2016 Effects of Cl-based ligand structures on atomic layer deposited HfO_2 *J. Phys. Chem.* C **120** 5958–67

[99] Zhao R, Guo Z and Wang X W 2018 Surface chemistry during atomic-layer deposition of nickel sulfide from nickel amidinate and H_2S *J. Phys. Chem.* C **122** 21514–20

[100] Siimon H and Aarik J 1997 Thickness profiles of thin films caused by secondary reactions in flow-type atomic layer deposition reactors *J. Phys. D: Appl. Phys.* **30** 1725–8

[101] Pilli A, Jones J, Lee V, Chugh N, Kelber J, Pasquale F and LaVoie A 2018 *In situ* XPS study of low temperature atomic layer deposition of B_2O_3 films on Si using BCl_3 and H_2O precursors *J. Vac. Sci. Technol.* A **36** 061503

[102] Zhao R, Xiao S, Yang S H and Wang X W 2019 Surface thermolytic behavior of nickel amidinate and its implication on the atomic layer deposition of nickel compounds *Chem. Mater.* **31** 5172–80

[103] Li H, Shao Y D, Su Y T, Gao Y H and Wang X W 2016 Vapor-phase atomic layer deposition of nickel sulfide and its application for efficient oxygen-evolution electrocatalysis *Chem. Mater.* **28** 1155–64

[104] Grillo F, Van Bui H, Moulijn J A, Kreutzer M T and Van Ommen J R 2017 Understanding and controlling the aggregative growth of platinum nanoparticles in atomic layer deposition: an avenue to size selection *J. Phys. Chem. Lett.* **8** 975–83

[105] Mackus A J M, Verheijen M A, Leick N, Bol A A and Kessels W M M 2013 Influence of oxygen exposure on the nucleation of platinum atomic layer deposition: consequences for film growth, nanopatterning, and nanoparticle synthesis *Chem. Mater.* **25** 1905–11

[106] Zhao R and Wang X W 2019 Initial growth and agglomeration during atomic layer deposition of nickel sulfide *Chem. Mater.* **31** 445–53

[107] Zhu J H, Zhao R, Shi J M, Wa Q B, Zhang M and Wang X W 2021 Metal exchange and diffusion during atomic layer deposition of cobalt and nickel sulfides *Chem. Mater.* **33** 9403–12

[108] Elam J W, Routkevitch D and George S M 2003 Properties of ZnO/Al_2O_3 alloy films grown using atomic layer deposition techniques *J. Electrochem. Soc.* **150** G339–47

[109] Elam J W, Libera J A, Pellin M J and Stair P C 2007 Spatially controlled atomic layer deposition in porous materials *Appl. Phys. Lett.* **91** 243105

[110] Bayer T J M, Wachau A, Fuchs A, Deuermeier J and Klein A 2012 Atomic layer deposition of Al_2O_3 onto Sn-Doped In_2O_3: absence of self-limited adsorption during initial growth by oxygen diffusion from the substrate and band offset modification by Fermi level pinning in Al_2O_3 *Chem. Mater.* **24** 4503–10

[111] George S M and Lee Y 2016 Prospects for thermal atomic layer etching using sequential, self-limiting fluorination and ligand-exchange reactions *ACS Nano* **10** 4889–94

[112] George S M 2020 Mechanisms of thermal atomic layer etching *Acc. Chem. Res.* **53** 1151–60

[113] Fischer A, Routzahn A, George S M and Lill T 2021 Thermal atomic layer etching: a review *J. Vac. Sci. Technol.* A **39** 030801

[114] Klesko J P, Kerrigan M M and Winter C H 2016 Low temperature thermal atomic layer deposition of cobalt metal films *Chem. Mater.* **28** 700–3

[115] Holden K E K, Dezelah C L and Conley J F 2019 Atomic layer deposition of transparent p-type semiconducting nickel oxide using $Ni(^{tBu2}DAD)_2$ and ozone *ACS Appl. Mater. Interfaces* **11** 30437–45

[116] Kim J *et al* 2017 Low-temperature atomic layer deposition of cobalt oxide as an effective catalyst for photoelectrochemical water-splitting devices *Chem. Mater.* **29** 5796–805

[117] Kerrigan M M, Klesko J P and Winter C H 2017 Low temperature, selective atomic layer deposition of cobalt metal films using Bis(1,4-di-tert-butyl-1,3-diazadienyl)cobalt and alkylamine precursors *Chem. Mater.* **29** 7458–66

[118] Maeng W J, Choi D W, Park J and Park J 2015 Indium oxide thin film prepared by low temperature atomic layer deposition using liquid precursors and ozone oxidant *J. Alloys Compd.* **649** 216–21

[119] Kim K, Lee K, Han S J, Park T, Lee Y, Kim J, Yeom S and Jeon H 2007 Comparison of co films deposited by remote plasma atomic layer deposition method with cyclopentadienylcobalt dicarbonyl $[CpCo(CO)_2]$ and dicobalt octacarbonyl $[Co_2(CO)_8]$ *Jpn. J. Appl. Phys.* **46** L173–6

[120] Leick N, Agarwal S, Mackus A J M and Kessels W M M 2012 Dehydrogenation reactions during atomic layer deposition of Ru using O_2 *Chem. Mater.* **24** 3696–700

[121] Bernal-Ramos K, Saly M J, Kanjolia R K and Chabal Y J 2015 Atomic layer deposition of cobalt silicide thin films studied by *in situ* infrared spectroscopy *Chem. Mater.* **27** 4943–9

[122] Bouman M and Zaera F 2016 Kinetics of adsorption of methylcyclopentadienyl manganese tricarbonyl on copper surfaces and implications for the atomic layer deposition of thin solid films *J. Phys. Chem.* C **120** 8232–9

[123] Gao Z N, Le D, Khaniya A, Dezelah C L, Woodruff J, Kanjolia R K, Kaden W E, Rahman T S and Banerjee P 2019 Self-catalyzed, low-temperature atomic layer deposition of ruthenium metal using zero-valent $Ru(DMBD)(CO)_3$ and water *Chem. Mater.* **31** 1304–17

[124] Kim T H, Nandi D K, Ramesh R, Han S M, Shong B and Kim S H 2019 Some insights into atomic layer deposition of MoN_x using $Mo(CO)_6$ and NH_3 and its diffusion barrier application *Chem. Mater.* **31** 8338–50

[125] Database of ALD processes (available at: www.atomiclimits.com/alddatabase/)

[126] Ritala M, Leskelä M, Nykänen E, Soininen P and Niinistö L 1993 Growth of titanium dioxide thin films by atomic layer epitaxy *Thin Solid Films* **225** 288–95

[127] Alén P, Ritala M, Arstila K, Keinonen J and Leskelä M 2005 The growth and diffusion barrier properties of atomic layer deposited NbN_x thin films *Thin Solid Films* **491** 235–41

[128] Rossnagel S M, Sherman A and Turner F 2000 Plasma-enhanced atomic layer deposition of Ta and Ti for interconnect diffusion barriers *J. Vac. Sci. Technol.* B **18** 2016–20

[129] Kim Y *et al* 2019 Synthesis of two-dimensional MoS_2/graphene heterostructure by atomic layer deposition using MoF_6 precursor *Appl. Surf. Sci.* **494** 591–9

[130] Klaus J W, Ferro S J and George S M 2000 Atomic layer deposition of tungsten using sequential surface chemistry with a sacrificial stripping reaction *Thin Solid Films* **360** 145–53

[131] Hwang Y H, Cho W J and Kim Y 2013 Investigation of tungsten nitride deposition using tungsten hexafluoride precursor for via and plug metallization *Jpn. J. Appl. Phys.* **52** 10MC07

[132] Ritala M and Leskelä M 1994 Zirconium dioxide thin films deposited by ale using zirconium tetrachloride as precursor *Appl. Surf. Sci.* **75** 333–40

[133] Ritala M, Leskelä M, Niinistö L, Prohaska T, Friedbacher G and Grasserbauer M 1994 Development of crystallinity

and morphology in hafnium dioxide thin films grown by atomic layer epitaxy *Thin Solid Films* **250** 72–80
[134] Pore V, Hatanpää T, Ritala M and Leskelä M 2009 Atomic layer deposition of metal tellurides and selenides using alkylsilyl compounds of tellurium and selenium *J. Am. Chem. Soc.* **131** 3478–80
[135] Kim O H, Kim D and Anderson T 2009 Atomic layer deposition of GaN using $GaCl_3$ and NH_3 *J. Vac. Sci. Technol.* A **27** 923–8
[136] Ihanus J, Lankinen M P, Kemell M, Ritala M and Leskelä M 2005 Aging of electroluminescent ZnS:Mn thin films deposited by atomic layer deposition processes *J. Appl. Phys.* **98** 113526
[137] Ott A W and Chang R P H 1999 Atomic layer-controlled growth of transparent conducting ZnO on plastic substrates *Mater. Chem. Phys.* **58** 132–8
[138] Bakke J R, Hägglund C, Jung H J, Sinclair R and Bent S F 2013 Atomic layer deposition of CdO and $Cd_xZn_{1-x}O$ films *Mater. Chem. Phys.* **140** 465–71
[139] Ott A W, Klaus J W, Johnson J M and George S M 1997 Al_3O_3 thin film growth on Si(100) using binary reaction sequence chemistry *Thin Solid Films* **292** 135–44
[140] Comstock D J and Elam J W 2012 Atomic layer deposition of Ga_2O_3 films using trimethylgallium and ozone *Chem. Mater.* **24** 4011–8
[141] Mane A U, Allen A J, Kanjolia R K and Elam J W 2016 Indium oxide thin films by atomic layer deposition using trimethylindium and ozone *J. Phys. Chem.* C **120** 9874–83
[142] Drozd V E and Aleskovski V B 1994 Synthesis of conducting oxides by ML-ALE *Appl. Surf. Sci.* **82–83** 591–4
[143] Burton B B, Goldstein D N and George S M 2009 Atomic layer deposition of MgO using Bis(ethylcyclopentadienyl)magnesium and H_2O *J. Phys. Chem.* C **113** 1939–46
[144] Holme T P and Prinz F B 2007 Atomic layer deposition and chemical vapor deposition precursor selection method application to strontium and barium precursors *J. Phys. Chem.* A **111** 8147–51
[145] Putkonen M, Nieminen M, Niinistö J, Niinistö L and Sajavaara T 2001 Surface-controlled deposition of Sc_2O_3 thin films by atomic layer epitaxy using β-diketonate and organometallic precursors *Chem. Mater.* **13** 4701–7
[146] Shim J H, Park J S, An J, Gür T M, Kang S and Prinz F B 2009 Intermediate-temperature ceramic fuel cells with thin film yttrium-doped barium zirconate electrolytes *Chem. Mater.* **21** 3290–6
[147] Burton B B, Fabreguette F H and George S M 2009 Atomic layer deposition of MnO using Bis(ethylcyclopentadienyl) manganese and H_2O *Thin Solid Films* **517** 5658–65
[148] Rooth M, Johansson A, Kukli K, Aarik J, Boman M and Hårsta A 2008 Atomic layer deposition of iron oxide thin films and nanotubes using ferrocene and oxygen as precursors *Chem. Vap. Depos.* **14** 67–70
[149] Diskus M, Nilsen O and Fjellvåg H 2011 Thin films of cobalt oxide deposited on high aspect ratio supports by atomic layer deposition *Chem. Vap. Depos.* **17** 135–40
[150] Bachmann J, Zolotaryov A, Albrecht O, Goetze S, Berger A, Hesse D, Novikov D and Nielsch K 2011 Stoichiometry of nickel oxide films prepared by ALD *Chem. Vap. Depos.* **17** 177–80
[151] Kwon O K, Kim J H, Park H S and Kang S W 2004 Atomic layer deposition of ruthenium thin films for copper glue layer *J. Electrochem. Soc.* **151** G109–12
[152] Elam J W, Martinson A B F, Pellin M J and Hupp J T 2006 Atomic layer deposition of In_2O_3 using cyclopentadienyl indium: a new synthetic route to transparent conducting oxide films *Chem. Mater.* **18** 3571–8
[153] Kozen A C, Pearse A J, Lin C F, Schroeder M A, Noked M, Lee S B and Rubloff G W 2014 Atomic layer deposition and *in situ* characterization of ultraclean lithium oxide and lithium hydroxide *J. Phys. Chem.* C **118** 27749–53
[154] Dufond M E, Diouf M W, Badie C, Laffon C, Parent P, Ferry D, Grosso D, Kools J C S, Elliott S D and Santinacci L 2020 Quantifying the extent of ligand incorporation and the effect on properties of TiO_2 thin films grown by atomic layer deposition using an alkoxide or an alkylamide *Chem. Mater.* **32** 1393–407
[155] Jeong D, Lee J and Kim J 2004 Effects of various oxidizers on the ZrO_2 thin films deposited by atomic layer deposition *Integr. Ferroelectr.* **67** 41–48
[156] Park H B, Cho M, Park J, Lee S W, Park T J and Hwang C S 2004 Improvements in reliability and leakage current properties of HfO_2 gate dielectric films by *in situ* O_3 oxidation of Si substrate *Electrochem. Solid-State Lett.* **7** G254–7
[157] Musschoot J, Deduytsche D, Poelman H, Haemers J, Van Meirhaeghe R L, Van Den Berghe S and Detavernier C 2009 Comparison of thermal and plasma-enhanced ALD/CVD of vanadium pentoxide *J. Electrochem. Soc.* **156** P122
[158] Kukli K, Ritala M and Leskelä M 1995 Atomic layer epitaxy growth of tantalum oxide thin films from $Ta(OC_2H_5)_5$ and H_2O *J. Electrochem. Soc.* **142** 1670–5
[159] Hashemi F S M, Cao L A, Mattelaer F, Sajavaara T, Van Ommen J R and Detavernier C 2019 Aluminum tri-isopropoxide as an alternative precursor for atomic layer deposition of aluminum oxide thin films *J. Vac. Sci. Technol.* A **37** 040901
[160] Hatanpää T, Ihanus J, Kansikas J, Mutikainen I, Ritala M and Leskelä M 1999 Properties of $[Mg_2(thd)_4]$ as a precursor for atomic layer deposition of MgO thin films and crystal structures of $[Mg_2(thd)_4]$ and $[Mg(thd)_2(EtOH)_2]$ *Chem. Mater.* **11** 1846–52
[161] Nilsen O, Fjellvåg H and Kjekshus A 2004 Growth of calcium carbonate by the atomic layer chemical vapour deposition technique *Thin Solid Films* **450** 240–7
[162] Nilsen O, Lie M, Foss S, Fjellvåg H and Kjekshus A 2004 Effect of magnetic field on the growth of α-Fe_2O_3 thin films by atomic layer deposition *Appl. Surf. Sci.* **227** 40–47
[163] Klepper K B, Nilsen O and Fjellvåg H 2007 Growth of thin films of Co_3O_4 by atomic layer deposition *Thin Solid Films* **515** 7772–81
[164] Niskanen A, Rahtu A, Sajavaara T, Arstila K, Ritala M and Leskela M 2005 Radical-enhanced atomic layer deposition of metallic copper thin films *J. Electrochem. Soc.* **152** G25–G28
[165] Aaltonen T, Ritala M, Tung Y L, Chi Y, Arstila K, Meinander K and Leskelä M 2004 Atomic layer deposition of noble metals: exploration of the low limit of the deposition temperature *J. Mater. Res.* **19** 3353–8
[166] Mattinen M, Hämäläinen J, Vehkamäki M, Heikkilä M J, Mizohata K, Jalkanen P, Räisänen J, Ritala M and Leskelä M 2016 Atomic layer deposition of iridium thin films using sequential oxygen and hydrogen pulses *J. Phys. Chem.* C **120** 15235–43
[167] Hämäläinen J, Munnik F, Ritala M and Leskelä M 2008 Atomic layer deposition of platinum oxide and metallic platinum thin films from $Pt(acac)_2$ and ozone *Chem. Mater.* **20** 6840–6
[168] Nieminen M, Putkonen M and Niinistö L 2001 Formation and stability of lanthanum oxide thin films deposited from β-diketonate precursor *Appl. Surf. Sci.* **174** 155–66
[169] Päiväsaari J, Putkonen M and Niinistö L 2002 Cerium dioxide buffer layers at low temperature by atomic layer deposition *J. Mater. Chem.* **12** 1828–32
[170] Päiväsaari J, Putkonen M and Niinistö L 2005 A comparative study on lanthanide oxide thin films grown by atomic layer deposition *Thin Solid Films* **472** 275–81

[171] Myllymäki P, Roeckerath M, Lopes J M, Schubert J, Mizohata K, Putkonen M and Niinistö L 2010 Rare earth scandate thin films by atomic layer deposition: effect of the rare earth cation size *J. Mater. Chem.* **20** 4207–12

[172] Hausmann D M, Kim E, Becker J and Gordon R G 2002 Atomic layer deposition of hafnium and zirconium oxides using metal amide precursors *Chem. Mater.* **14** 4350–8

[173] Kukli K, Ritala M, Lu J, Harsta A and Leskela M 2004 Properties of HfO_2 thin films grown by ALD from hafnium tetrakis(ethylmethylamide) and water *J. Electrochem. Soc.* **151** F189–93

[174] Zhao R, Gao Y H, Guo Z, Su Y T and Wang X W 2017 Interface energy alignment of atomic-layer-deposited VO_x on pentacene: an *in situ* photoelectron spectroscopy investigation *ACS Appl. Mater. Interfaces* **9** 1885–90

[175] Maeng W J and Kim H 2006 Thermal and plasma-enhanced ALD of Ta and Ti oxide thin films from alkylamide precursors *Electrochem. Solid-State Lett.* **9** G191–4

[176] Dezelah C L, Niinistö J, Arstila K, Niinistö L and Winter C H 2006 Atomic layer deposition of Ga_2O_3 films from a dialkylamido-based precursor *Chem. Mater.* **18** 471–5

[177] Elam J W, Baker D A, Hryn A J, Martinson A B F, Pellin M J and Hupp J T 2008 Atomic layer deposition of tin oxide films using tetrakis(dimethylamino) tin *J. Vac. Sci. Technol.* A **26** 244–52

[178] Burton B B, Kang S W, Rhee S W and George S M 2009 SiO_2 atomic layer deposition using tris(dimethylamino)silane and hydrogen peroxide studied by *in situ* transmission FTIR spectroscopy *J. Phys. Chem.* C **113** 8249–57

[179] Yoon C M *et al* 2018 Water-erasable memory device for security applications prepared by the atomic layer deposition of GeO_2 *Chem. Mater.* **30** 830–40

[180] Kim S B, Yang C X, Powers T, Davis L M, Lou X B and Gordon R G 2016 Synthesis of calcium(II) amidinate precursors for atomic layer deposition through a redox reaction between calcium and amidines *Angew. Chem., Int. Ed.* **55** 10228–33

[181] De Rouffignac P, Yousef A P, Kim K H and Gordon R G 2006 ALD of scandium oxide from scandium Tris(*N, N′*-diisopropylacetamidinate) and water *Electrochem. Solid-State Lett.* **9** F45–F48

[182] De Rouffignac P, Park J S and Gordon R G 2005 Atomic layer deposition of Y_2O_3 thin films from yttrium tris(*N,N′*-diisopropylacetamidinate) and water *Chem. Mater.* **17** 4808–14

[183] Weimer M S, Kim I S, Guo P J, Schaller R D, Martinson A B F and Hock A S 2017 Oxidation state discrimination in the atomic layer deposition of vanadium oxides *Chem. Mater.* **29** 6238–44

[184] Du L Y, Yu S S, Liu X F and Ding Y Q 2019 An efficient atomic layer deposition process of MnO_x films using bis(*N,N′*-di-tert-butylacetamidinato)manganese-(II) and H_2O as reactants *Appl. Surf. Sci.* **486** 460–5

[185] Li H, Gao Y H, Shao Y D, Su Y T and Wang X W 2015 Vapor-phase atomic layer deposition of Co_9S_8 and its application for supercapacitors *Nano Lett.* **15** 6689–95

[186] Guo Z, Li H, Chen Q, Sang L J, Yang L Z, Liu Z W and Wang X W 2015 Low-temperature atomic layer deposition of high purity, smooth, low resistivity copper films by using amidinate precursor and hydrogen plasma *Chem. Mater.* **27** 5988–96

[187] Kim S B, Jayaraman A, Chua D, Davis L M, Zheng S L, Zhao X Z, Lee S and Gordon R G 2018 Obtaining a low and wide atomic layer deposition window (150–275 °C) for In_2O_3 films using an In^{III} amidinate and H_2O *Eur. J. Chem.* **24** 9525–9

[188] Huster N, Ghiyasi R, Zanders D, Rogalla D, Karppinen M and Devi A 2022 SnO deposition *via* water based ALD employing tin(II) formamidinate: precursor characterization and process development *Dalton Trans.* **51** 14970–9

[189] Du L Y, Wang K Y, Zhong Y P, Liu B, Liu X F and Ding Y Q 2020 A high growth rate process of ALD CeO_x with amidinato-cerium [(N-^{i}Pr-AMD)$_3$Ce] and O_3 as precursors *J. Mater. Sci.* **55** 5378–89

[190] De Rouffignac P and Gordon R G 2006 Atomic layer deposition of praseodymium aluminum oxide for electrical applications *Chem. Vap. Depos.* **12** 152–7

[191] Kim K H, Farmer D B, Lehn J S M, Rao P V and Gordon R G 2006 Atomic layer deposition of gadolinium scandate films with high dielectric constant and low leakage current *Appl. Phys. Lett.* **89** 133512

[192] Paivasaari J, Dezelah I V C L, Back D, El-Kaderi H M, Heeg M J, Putkonen M, Niinisto L and Winter C H 2005 Synthesis, structure and properties of volatile lanthanide complexes containing amidinate ligands: application for Er_2O_3 thin film growth by atomic layer deposition *J. Mater. Chem.* **15** 4224–33

[193] Wang H T, Wang J J, Gordon R, Lehn J S M, Li H Z, Hong D and Shenai D V 2009 Atomic layer deposition of lanthanum-based ternary oxides *Electrochem. Solid-State Lett.* **12** G13–G15

[194] Potts S E, Dingemans G, Lachaud C and Kessels W M M 2012 Plasma-enhanced and thermal atomic layer deposition of Al_2O_3 using dimethylaluminum isopropoxide, $[Al(CH_3)_2(\mu\text{-}O^iPr)]_2$, as an alternative aluminum precursor *J. Vac. Sci. Technol.* A **30** 021505

[195] Putkonen M and Niinistö L 2001 Zirconia thin films by atomic layer epitaxy. A comparative study on the use of novel precursors with ozone *J. Mater. Chem.* **11** 3141–7

[196] Niinistö J, Putkonen M, Niinistö L, Arstila K, Sajavaara T, Lu J, Kukli K, Ritala M and Leskelä M 2006 HfO_2 films grown by ALD using cyclopentadienyl-type precursors and H_2O or O_3 as oxygen source *J. Electrochem. Soc.* **153** F39–F45

[197] Klesko J P *et al* 2018 Selective atomic layer deposition mechanism for titanium dioxide films with $(EtCp)Ti(NMe_2)_3$: ozone versus water *Chem. Mater.* **30** 970–81

[198] Seppälä S, Niinistö J, Blanquart T, Kaipio M, Mizohata K, Räisänen J, Lansalot-Matras C, Noh W, Ritala M and Leskelä M 2016 Heteroleptic cyclopentadienyl-amidinate precursors for atomic layer deposition (ALD) of Y, Pr, Gd, and Dy oxide thin films *Chem. Mater.* **28** 5440–9

[199] Seppälä S, Niinistö J, Mattinen M, Mizohata K, Räisänen J, Noh W, Ritala M and Leskelä M 2018 Atomic layer deposition of lanthanum oxide with heteroleptic cyclopentadienyl-amidinate lanthanum precursor—effect of the oxygen source on the film growth and properties *Thin Solid Films* **660** 199–206

[200] Kim J M, Lee H B R, Lansalot C, Dussarrat C, Gatineau J and Kim H 2010 Plasma-enhanced atomic layer deposition of cobalt using cyclopentadienyl isopropyl acetamidinato-cobalt as a precursor *Jpn. J. Appl. Phys.* **49** 05FA10

[201] Knoops H C M, Baggetto L, Langereis E, Van De Sanden M C M, Klootwijk J H, Roozeboom F, Niessen R A H, Notten P H L and Kessels W M M 2008 Deposition of TiN and TaN by remote plasma ALD for Cu and Li diffusion barrier applications *J. Electrochem. Soc.* **155** G287–94

[202] Aarik J, Aidla A, Kiisler A A, Uustare T and Sammelselg V 1999 Influence of substrate temperature on atomic layer growth and properties of HfO_2 thin films *Thin Solid Films* **340** 110–6

[203] Park H B, Cho M, Park J, Lee S W, Hwang C S and Jeongb J 2004 Optimized nitridation of Al_2O_3 interlayers for

atomic-layer-deposited HfO_2 gate dielectric films *Electrochem. Solid-State Lett.* **7** F25–F29
[204] Triyoso D H *et al* 2004 Film properties of ALD HfO_2 and La_2O_3 gate dielectrics grown on Si with various pre-deposition treatments *J. Vac. Sci. Technol.* B **22** 2121–7
[205] Törndahl T, Ottosson M and Carlsson J O 2004 Growth of copper metal by atomic layer deposition using copper(I) chloride, water and hydrogen as precursors *Thin Solid Films* **458** 129–36
[206] Asikainen T, Ritala M and Leskelä M 1994 Growth of In_2S_3 thin films by atomic layer epitaxy *Appl. Surf. Sci.* **82–83** 122–5
[207] Creighton J R 1989 A mechanism for selectivity loss during tungsten CVD *J. Electrochem. Soc.* **136** 271–6
[208] Szeghalmi A, Helgert M, Brunner R, Heyroth F, Gösele U and Knez M 2010 Tunable guided-mode resonance grating filter *Adv. Funct. Mater.* **20** 2053–62
[209] Kim J B, Kwon D R, Chakrabarti K, Lee C, Oh K Y and Lee J H 2002 Improvement in Al_2O_3 dielectric behavior by using ozone as an oxidant for the atomic layer deposition technique *J. Appl. Phys.* **92** 6739–42
[210] Kim S K, Lee S W, Hwang C S, Min Y S, Won J Y and Jeong J 2006 Low temperature ($<100\ ^\circ$C) deposition of aluminum oxide thin films by ALD with O_3 as oxidant *J. Electrochem. Soc.* **153** F69–F76
[211] Hoex B, Heil S B S, Langereis E, Van De Sanden M C M and Kessels W M M 2006 Ultralow surface recombination of *c*-Si substrates passivated by plasma-assisted atomic layer deposited Al_2O_3 *Appl. Phys. Lett.* **89** 042112
[212] Liu X Y, Zhao S X, Zhang L Q, Huang H F, Shi J S, Zhang C M, Lu H L, Wang P F and Zhang D W 2015 AlGaN/GaN MISHEMTs with AlN gate dielectric grown by thermal ALD technique *Nanoscale Res. Lett.* **10** 109
[213] Ishii M, Iwai S, Ueki T and Aoyagi Y 1998 Surface reaction mechanism and morphology control in AlP atomic layer epitaxy *Thin Solid Films* **318** 6–10
[214] Hirose S, Yoshida A, Yamaura M, Kano N and Munekata H 2000 Control of carbon incorporation in AlAs grown by atomic layer epitaxy using variously orientated substrates *J. Mater. Sci., Mater. Electron.* **11** 7–10
[215] Zafar M, Kim B and Kim D H 2019 Improvement in performance of inverted polymer solar cells by interface engineering of ALD ZnS on ZnO electron buffer layer *Appl. Surf. Sci.* **481** 1442–8
[216] Yokoyama M, Chen N T and Ueng H Y 2000 Growth and characterization of ZnSe on Si by atomic layer epitaxy *J. Cryst. Growth* **212** 97–102
[217] Wang W S, Ehsani H and Bhat I 1993 Improved CdTe layers on GaAs and Si using atomic layer epitaxy *J. Electron. Mater.* **22** 873–8
[218] Wheeler V D *et al* 2020 Phase control of crystalline Ga_2O_3 films by plasma-enhanced atomic layer deposition *Chem. Mater.* **32** 1140–52
[219] Lim J W, Kim T, Kim J, Yun S J, Jung K H and Park M A 2021 Photoinduced synaptic behavior of In_xTi_yO thin film transistors *Adv. Electron. Mater.* **7** 2001049
[220] Wang B W, Choi J, Kim H G, Hyun S D, Yoo C, Kim S, Lee H and Hwang C S 2021 Influences of oxygen source and substrate temperature on the unusual growth mechanism of atomic layer deposited magnesium oxide using bis(cyclopentadienyl)magnesium precursor *J. Mater. Chem.* C **9** 15359–74
[221] Lee W, Han J H, Jeon W, Yoo Y W, Lee S W, Kim S K, Ko C H, Lansalot-Matras C and Hwang C S 2013 Atomic layer deposition of $SrTiO_3$ films with cyclopentadienyl-based precursors for metal-insulator-metal capacitors *Chem. Mater.* **25** 953–61
[222] Vehkamäki M, Hänninen T, Ritala M, Leskelä M, Sajavaara T, Rauhala E and Keinonen J 2001 Atomic layer deposition of $SrTiO_3$ thin films from a novel strontium precursor-strontium-bis(tri-isopropyl cyclopentadienyl) *Chem. Vap. Depos.* **7** 75–80
[223] Ihanus J, Hänninen T, Hatanpää T, Aaltonen T, Mutikainen I, Sajavaara T, Keinonen J, Ritala M and Leskelä M 2002 Atomic layer deposition of SrS and BaS thin films using cyclopentadienyl precursors *Chem. Mater.* **14** 1937–44
[224] Kim W S, Park S K, Moon D Y, Kang B W, Kim H D and Park J W 2009 Characteristics of La_2O_3 thin films deposited using the ECR atomic layer deposition method *J. Korean Phys. Soc.* **55** 590–3
[225] Shin J W, Oh S, Lee S, Yu J G, Park J, Go D, Yang B C, Kim H J and An J 2019 Ultrathin atomic layer-deposited CeO_2 overlayer for high-performance fuel cell electrodes *ACS Appl. Mater. Interfaces* **11** 46651–7
[226] Liu J, Lu H L, Zhang D W and Nolan M 2022 Self-limiting nitrogen/hydrogen plasma radical chemistry in plasma-enhanced atomic layer deposition of cobalt *Nanoscale* **14** 4712–25
[227] Hufnagel A G, Henß A K, Hoffmann R, Zeman O E O, Häringer S, Fattakhova-Rohlfing D and Bein T 2018 Electron-blocking and oxygen evolution catalyst layers by plasma-enhanced atomic layer deposition of nickel oxide *Adv. Mater. Interfaces* **5** 1701531
[228] Lu H L, Scarel G, Wiemer C, Perego M, Spiga S, Fanciulli M and Pavia G 2008 Atomic layer deposition of NiO films on Si(100) using cyclopentadienyl-type compounds and ozone as precursors *J. Electrochem. Soc.* **155** H807–11
[229] Chae J, Park H S and Kang S W 2002 Atomic layer deposition of nickel by the reduction of preformed nickel oxide *Electrochem. Solid-State Lett.* **5** C64–C66
[230] Oh I K, Kim H and Lee H B R 2017 Growth mechanism of Co thin films formed by plasma-enhanced atomic layer deposition using NH_3 as plasma reactant *Curr. Appl. Phys.* **17** 333–8
[231] Vos M F J, Van Straaten G, Kessels W M M E and Mackus A J M 2018 Atomic layer deposition of cobalt using H_2-, N_2-, and NH_3–based plasmas: on the role of the Co-reactant *J. Phys. Chem.* C **122** 22519–29
[232] Aaltonen T, Rahtu A, Ritala M and Leskelä M 2003 Reaction mechanism studies on atomic layer deposition of ruthenium and platinum *Electrochem. Solid-State Lett.* **6** C130–3
[233] Hämäläinen J, Hatanpää T, Puukilainen E, Costelle L, Pilvi T, Ritala M and Leskelä M 2010 (MeCp)Ir(CHD) and molecular oxygen as precursors in atomic layer deposition of iridium *J. Mater. Chem.* **20** 7669–75
[234] Ma Q, Zheng H M, Shao Y, Zhu B, Liu W J, Ding S J and Zhang D W 2018 Atomic-layer-deposition of indium oxide nano-films for thin-film transistors *Nanoscale Res. Lett.* **13** 4
[235] Rahtu A and Ritala M 2002 Reaction mechanism studies on titanium isopropoxide-water atomic layer deposition process *Chem. Vap. Depos.* **8** 21–28
[236] Piszczek P, Radtke A, Muzioł T, Richert M and Chojnacki J 2012 The conversion of multinuclear μ-oxo titanium(IV) species in the reaction of $Ti(O^iBu)_4$ with branched organic acids; results of structural and spectroscopic studies *Dalton Trans.* **41** 8261–9
[237] Pore V, Rahtu A, Leskelä M, Ritala M, Sajavaara T and Keinonen J 2004 Atomic layer deposition of photocatalytic TiO_2 thin films from titanium tetramethoxide and water *Chem. Vap. Depos.* **10** 143–8
[238] Chaukulkar R P and Agarwal S 2013 Atomic layer deposition of titanium dioxide using titanium tetrachloride and titanium tetraisopropoxide as precursors *J. Vac. Sci. Technol.* A **31** 031509

[239] Putkonen M, Sajavaara T, Johansson L S and Niinistö L 2001 Low-temperature ALE deposition of Y_2O_3 thin films from β-diketonate precursors *Chem. Vap. Depos.* **7** 44–50

[240] Hanninen T, Mutikainen I, Saanila V, Ritala M, Leskela M and Hanson J C 1997 [Ca(Thd)$_2$(tetraen)]: a monomeric precursor for deposition of CaS thin films *Chem. Mater.* **9** 1234–40

[241] Van T T and Chang J P 2005 Surface reaction kinetics of metal β-diketonate precursors with O radicals in radical-enhanced atomic layer deposition of metal oxides *Appl. Surf. Sci.* **246** 250–61

[242] Putkonen M, Johansson L S, Rauhala E and Niinistö L 1999 Surface-controlled growth of magnesium oxide thin films by atomic layer epitaxy *J. Mater. Chem.* **9** 2449–52

[243] Putkonen M, Sajavaara T, Rahkila P, Xu L T, Cheng S L, Niinistö L and Whitlow H J 2009 Atomic layer deposition and characterization of biocompatible hydroxyapatite thin films *Thin Solid Films* **517** 5819–24

[244] Kosola A, Putkonen M, Johansson L S and Niinistö L 2003 Effect of annealing in processing of strontium titanate thin films by ALD *Appl. Surf. Sci.* **211** 102–12

[245] Torndahl T, Ottosson M and Carlsson J O 2006 Growth of copper(I) nitride by ALD using copper(II) hexafluoroacetylacetonate, water, and ammonia as precursors *J. Electrochem. Soc.* **153** C146–51

[246] Singh R and Ayyub M M 2021 Atomic layer deposition of crystalline β-NiS for superior sensing in thin-film non-enzymatic electrochemical glucose sensors *ACS Appl. Electron. Mater.* **3** 1912–9

[247] Mahuli N, Saha D and Sarkar S K 2017 Atomic layer deposition of p-type Bi_2S_3 *J. Phys. Chem.* C **121** 8136–44

[248] Sarkar S K, Kim J Y, Goldstein D N, Neale N R, Zhu K, Elliot C M, Frank A J and George S M 2010 In_2S_3 atomic layer deposition and its application as a sensitizer on TiO_2 nanotube arrays for solar energy conversion *J. Phys. Chem.* C **114** 8032–9

[249] Aarik J, Aidla A, Jaek A, Leskelä M and Niinistö L 1994 Precursor properties of calcium β-diketonate in vapor phase atomic layer epitaxy *Appl. Surf. Sci.* **75** 33–38

[250] Park N K, Kang D K, Kim B H, Jo S J and Ha J S 2006 Electrical properties of La_2O_3 thin films grown on TiN/Si substrates via atomic layer deposition *Appl. Surf. Sci.* **252** 8506–9

[251] Kukli K, Peussa M, Johansson L S, Nykänen E and Niinistö L 1999 Controlled growth of yttrium oxysulphide thin films by atomic layer deposition *Mater. Sci. Forum* **315–317** 216–21

[252] Feng H, Elam J W, Libera J A, Setthapun W and Stair P C 2010 Palladium catalysts synthesized by atomic layer deposition for methanol decomposition *Chem. Mater.* **22** 3133–42

[253] Tripathi T S, Wilken M, Hoppe C, De Los Arcos T, Grundmeier G, Devi A and Karppinen M 2021 Atomic layer deposition of copper metal films from Cu(acac)$_2$ and hydroquinone reductant *Adv. Eng. Mater.* **23** 2100446

[254] Pilvi T, Hatanpää T, Puukilainen E, Arstila K, Bischoff M, Kaiser U, Kaiser N, Leskelä M and Ritala M 2007 Study of a novel ALD process for depositing MgF_2 thin films *J. Mater. Chem.* **17** 5077–83

[255] Biercuk M J, Monsma D J, Marcus C M, Becker J S and Gordon R G 2003 Low-temperature atomic-layer-deposition lift-off method for microelectronic and nanoelectronic applications *Appl. Phys. Lett.* **83** 2405–7

[256] Gao Y H, Shao Y D, Yan L J, Li H, Su Y T, Meng H and Wang X W 2016 Efficient charge injection in organic field-effect transistors enabled by low-temperature atomic layer deposition of ultrathin VO_x interlayer *Adv. Funct. Mater.* **26** 4456–63

[257] Wang X W, Guo Z, Gao Y H and Wang J 2017 Atomic layer deposition of vanadium oxide thin films from tetrakis(dimethylamino)vanadium precursor *J. Mater. Res.* **32** 37–44

[258] Ansari M Z, Janicek P, Nandi D K, Slang S, Bouska M, Oh H, Shong B and Kim S H 2021 Low-temperature growth of crystalline Tin(II) monosulfide thin films by atomic layer deposition using a liquid divalent tin precursor *Appl. Surf. Sci.* **565** 150152

[259] Hong T E *et al* 2015 Highly conformal amorphous W-Si-N thin films by plasma-enhanced atomic layer deposition as a diffusion barrier for Cu metallization *J. Phys. Chem.* C **119** 1548–56

[260] Kim S B, Sinsermsuksakul P, Hock A S, Pike R D and Gordon R G 2014 Synthesis of N-heterocyclic stannylene (Sn(II)) and germylene (Ge(II)) and a Sn(II) amidinate and their application as precursors for atomic layer deposition *Chem. Mater.* **26** 3065–73

[261] Chen Z X, Li X, Li W M and Lo G Q 2016 Plasma-enhanced atomic layer deposition (PEALD) of TiN using the organic precursor tetrakis(ethylmethylamido)titanium (TEMAT) *MATEC Web Conf.* **39** 01010

[262] Rouf P, O'Brien N J, Buttera S C, Martinovic I, Bakhit B, Martinsson E, Palisaitis J, Hsu C W and Pedersen H 2020 Epitaxial GaN using Ga(NMe$_2$)$_3$ and NH_3 plasma by atomic layer deposition *J. Mater. Chem.* C **8** 8457–65

[263] Østreng E, Vajeeston P, Nilsen O and Fjellvåg H 2012 Atomic layer deposition of lithium nitride and carbonate using lithium silylamide *RSC Adv.* **2** 6315–22

[264] Wang T and Ekerdt J G 2010 Subnanoscale lanthanum distribution in lanthanum-incorporated hafnium oxide thin films grown using atomic layer deposition *Chem. Mater.* **22** 3798–806

[265] Nam W H and Rhee S W 2004 Atomic layer deposition of ZrO_2 thin films using dichlorobis[bis-(trimethylsilyl)amido]zirconium and water *Chem. Vap. Depos.* **10** 201–5

[266] Popov G, Mattinen M, Hatanpää T, Vehkamäki M, Kemell M, Mizohata K, Räisänen J, Ritala M and Leskelä M 2019 Atomic layer deposition of PbI_2 thin films *Chem. Mater.* **31** 1101–9

[267] Wan Z X, Zhang T F, Zeng Z H and Xi B 2022 Atomic layer deposition of Co_xO_y films: oxidants versus composition *Adv. Mater. Interfaces* **9** 2200097

[268] Guo Z, Zhao R, Yan S H, Xiong W, Zhu J H, Lu K and Wang X W 2021 Atomic layer deposition of $FeSe_2$, $CoSe_2$, and $NiSe_2$ *Chem. Mater.* **33** 2478–87

[269] Shao Y D, Guo Z, Li H, Su Y T and Wang X W 2017 Atomic layer deposition of iron sulfide and its application as a catalyst in the hydrogenation of azobenzenes *Angew. Chem., Int. Ed.* **56** 3226–31

[270] Wang X W, Dong L, Zhang J Y, Liu Y Q, Ye P D D and Gordon R G 2013 Heteroepitaxy of La_2O_3 and $La_{2-x}Y_xO_3$ on GaAs (111)A by atomic layer deposition: achieving low interface trap density *Nano Lett.* **13** 594–9

[271] Lee B *et al* 2009 Electrical properties of atomic-layer-deposited La_2O_3 films using a novel La formamidinate precursor and ozone *Microelectron. Eng.* **86** 1658–61

[272] Blanquart T, Niinistö J, Ritala M and Leskelä M 2014 Atomic layer deposition of groups 4 and 5 transition metal oxide thin films: focus on heteroleptic precursors *Chem. Vap. Depos.* **20** 189–208

[273] Niinistö J *et al* 2008 Novel mixed alkylamido-cyclopentadienyl precursors for ALD of ZrO_2 thin films *J. Mater. Chem.* **18** 5243–7

[274] Niinistö J, Mäntymäki M, Kukli K, Costelle L, Puukilainen E, Ritala M and Leskelä M 2010 Growth and

phase stabilization of HfO_2 thin films by ALD using novel precursors *J. Cryst. Growth* **312** 245–9
[275] Elam J W, Schuisky M, Ferguson J D and George S M 2003 Surface chemistry and film growth during TiN atomic layer deposition using TDMAT and NH_3 *Thin Solid Films* **436** 145–56
[276] Burton B B, Lavoie A R and George S M 2008 Tantalum nitride atomic layer deposition using (tert-butylimido) tris(diethylamido) tantalum and hydrazine *J. Electrochem. Soc.* **155** D508–16
[277] Musschoot J, Xie Q, Deduytsche D, Van Den Berghe S, Van Meirhaeghe R L and Detavernier C 2009 Atomic layer deposition of titanium nitride from TDMAT precursor *Microelectron. Eng.* **86** 72–77
[278] Kim H, Detavernier C, Van Der Straten O, Rossnagel S M, Kellock A J and Park D G 2005 Robust TaN_x diffusion barrier for Cu-interconnect technology with subnanometer thickness by metal-organic plasma-enhanced atomic layer deposition *J. Appl. Phys.* **98** 014308
[279] Kim D H, Kim Y J, Park J H and Kim J H 2004 Preparation of TiN films by plasma assisted atomic layer deposition for copper metallization *Mater. Sci. Eng.* C **24** 289–91
[280] Li H, Zhao R, Zhu J H, Guo Z, Xiong W and Wang X W 2020 Organosulfur precursor for atomic layer deposition of high-quality metal sulfide films *Chem. Mater.* **32** 8885–94
[281] Park H H 2021 Inorganic materials by atomic layer deposition for perovskite solar cells *Nanomaterials* **11** 88
[282] Hossain M A, Khoo K T, Cui X, Poduval G K, Zhang T, Li X, Li W M and Hoex B 2020 Atomic layer deposition enabling higher efficiency solar cells: a review *Nano Mater. Sci.* **2** 204–26
[283] Niu W B, Li X L, Karuturi S K, Fam D W, Fan H J, Shrestha S, Wong L H and Tok A I Y 2015 Applications of atomic layer deposition in solar cells *Nanotechnology* **26** 064001
[284] Raiford J A, Oyakhire S T and Bent S F 2020 Applications of atomic layer deposition and chemical vapor deposition for perovskite solar cells *Energy Environ. Sci.* **13** 1997–2023
[285] Wang X R and Yushin G 2015 Chemical vapor deposition and atomic layer deposition for advanced lithium ion batteries and supercapacitors *Energy Environ. Sci.* **8** 1889–904
[286] Li Z D, Su J J and Wang X D 2021 Atomic layer deposition in the development of supercapacitor and lithium-ion battery devices *Carbon* **179** 299–326
[287] Zhao Y *et al* 2021 Atomic/molecular layer deposition for energy storage and conversion *Chem. Soc. Rev.* **50** 3889–956
[288] Fonseca J and Lu J L 2021 Single-atom catalysts designed and prepared by the atomic layer deposition technique *ACS Catal.* **11** 7018–59
[289] Cao K, Cai J M, Liu X and Chen R 2018 Review article: catalysts design and synthesis via selective atomic layer deposition *J. Vac. Sci. Technol.* A **36** 010801
[290] Maina J W, Merenda A, Weber M, Pringle J M, Bechelany M, Hyde L and Dumée L F 2021 Atomic layer deposition of transition metal films and nanostructures for electronic and catalytic applications *Crit. Rev. Solid State Mater. Sci.* **46** 468–89
[291] Si M W, Lin Z H, Chen Z Z, Sun X, Wang H Y and Ye P D 2022 Scaled indium oxide transistors fabricated using atomic layer deposition *Nat. Electron.* **5** 164–70
[292] Sheng J Z, Choi D W, Lee S H, Park J and Park J 2016 Performance modulation of transparent ALD indium oxide films on flexible substrates: transition between metal-like conductor and high performance semiconductor states *J. Mater. Chem.* C **4** 7571–6
[293] Kim H Y *et al* 2016 Low-temperature growth of indium oxide thin film by plasma-enhanced atomic layer deposition using liquid dimethyl (N-ethoxy-2,2-dimethylpropanamido)indium for high-mobility thin film transistor application *ACS Appl. Mater. Interfaces* **8** 26924–31
[294] Sheng J Z, Park E J, Shong B and Park J S 2017 Atomic layer deposition of an indium gallium oxide thin film for thin-film transistor applications *ACS Appl. Mater. Interfaces* **9** 23934–40
[295] Hong T, Jeong H J, Lee H M, Choi S H, Lim J H and Park J S 2021 Significance of pairing In/Ga precursor structures on PEALD $InGaO_x$ thin-film transistor *ACS Appl. Mater. Interfaces* **13** 28493–502
[296] Seul H J, Kim M J, Yang H J, Cho M H, Cho M H, Song W B and Jeong J K 2020 Atomic layer deposition process-enabled carrier mobility boosting in field-effect transistors through a nanoscale ZnO/IGO heterojunction *ACS Appl. Mater. Interfaces* **12** 33887–98
[297] Baek I H, Pyeon J J, Han S H, Lee G Y, Choi B J, Han J H, Chung T M, Hwang C S and Kim S K 2019 High-performance thin-film transistors of quaternary indium-zinc-tin oxide films grown by atomic layer deposition *ACS Appl. Mater. Interfaces* **11** 14892–901
[298] Cho M H, Choi C H, Seul H J, Cho H C and Jeong J K 2021 Achieving a low-voltage, high-mobility IGZO transistor through an ALD-derived bilayer channel and a hafnia-based gate dielectric stack *ACS Appl. Mater. Interfaces* **13** 16628–40
[299] Cho M H, Seol H, Song A, Choi S, Song Y, Yun P S, Chung K B, Bae J U, Park K S and Jeong J K 2019 Comparative study on performance of IGZO transistors with sputtered and atomic layer deposited channel layer *IEEE Trans. Electron Devices* **66** 1783–8
[300] Li J Y, Zhang Y Q, Wang J L, Yang H, Zhou X L, Chan M S, Wang X W, Lu L and Zhang S D 2022 High-performance self-aligned top-gate amorphous InGaZnO TFTs with 4 nm-thick atomic-layer-deposited AlO_x insulator *IEEE Electron Device Lett.* **43** 729–32
[301] Böscke T S, Müller J, Bräuhaus D, Schröder U and Böttger U 2011 Ferroelectricity in hafnium oxide thin films *Appl. Phys. Lett.* **99** 102903
[302] Cheema S S *et al* 2020 Enhanced ferroelectricity in ultrathin films grown directly on silicon *Nature* **580** 478–82
[303] Luo Q *et al* 2020 A highly CMOS compatible hafnia-based ferroelectric diode *Nat. Commun.* **11** 1391
[304] Mulaosmanovic H, Ocker J, Müller S, Schroeder U, Müller J, Polakowski P, Flachowsky S, Van Bentum R, Mikolajick T and Slesazeck S 2017 Switching kinetics in nanoscale hafnium oxide based ferroelectric field-effect transistors *ACS Appl. Mater. Interfaces* **9** 3792–8
[305] Chen W C, Huang F, Qin S, Yu Z, Lin Q, McIntyre P C, Wong S S and Wong H S P 2022 4 bits/cell hybrid 1F1R for high density embedded non-volatile memory and its application for compute in memory *2022 IEEE Symposium on VLSI Technology and Circuits* (Honolulu, HI: IEEE) pp 244–5
[306] Lee M H and Shue W S 2020 The overview of current interconnect technology challenges and future opportunities *2020 IEEE International Electron Devices Meeting (IEDM)* (San Francisco, CA: IEEE) pp 32.1.1–32.1.4
[307] Kim H W 2022 Recent trends in copper metallization *Electronics* **11** 2914
[308] Park J S, Lee M J, Lee C S and Kang S W 2001 Plasma-enhanced atomic layer deposition of tantalum nitrides using hydrogen radicals as a reducing agent *Electrochem. Solid-State Lett.* **4** C17–C19
[309] Kim H and Rossnagel S M 2003 Plasma-enhanced atomic layer deposition of tantalum thin films: the growth and film properties *Thin Solid Films* **441** 311–6

[310] Wu L and Eisenbraun E 2009 Integration of atomic layer deposition-grown copper seed layers for Cu electroplating applications *J. Electrochem. Soc.* **156** H734–9
[311] Park J H, Moon D Y, Han D S, Kang Y J, Shin S R, Jeon H T and Park J W 2014 Plasma-enhanced atomic layer deposition (PEALD) of cobalt thin films for copper direct electroplating *Surf. Coat. Technol.* **259** 98–101
[312] Witt C, Yeap K B, Leśniewska A, Wan D, Jordan N, Ciofi I, Wu C and Tokei Z 2018 Testing the limits of TaN barrier scaling *2018 IEEE International Interconnect Technology Conference (IITC)* (Santa Clara, CA: IEEE) pp 54–56
[313] Torazawa N, Hirao S, Kanayama S, Korogi H and Matsumoto S 2016 The development of Cu filling and reliability performance with Ru-Ta alloy barrier for Cu interconnects *J. Electrochem. Soc.* **163** E173–8
[314] Swerts J *et al* 2012 Scalability of plasma enhanced atomic layer deposited ruthenium films for interconnect applications *J. Vac. Sci. Technol.* A **30** 01A103
[315] Nogami T *et al* 2022 Advanced BEOL materials, processes, and integration to reduce line resistance of damascene Cu, Co, and subtractive Ru interconnects *2022 IEEE Symposium on VLSI Technology and Circuits (VLSI Technology and Circuits)* (Honolulu, HI: IEEE) pp 423–4
[316] Kim J Y, Seo S, Kim D Y, Jeon H and Kim Y 2004 Remote plasma enhanced atomic layer deposition of TiN thin films using metalorganic precursor *J. Vac. Sci. Technol.* A **22** 8–12
[317] Muñoz-Rojas D, Maindron T, Esteve A, Piallat F, Kools J C S and Decams J M 2019 Speeding up the unique assets of atomic layer deposition *Mater. Today Chem.* **12** 96–120
[318] Poodt P, Cameron D C, Dickey E, George S M, Kuznetsov V, Parsons G N, Roozeboom F, Sundaram G and Vermeer A 2012 Spatial atomic layer deposition: a route towards further industrialization of atomic layer deposition *J. Vac. Sci. Technol.* A **30** 010802
[319] Hoye R L Z, Muñoz-Rojas D, Nelson S F, Illiberi A, Poodt P, Roozeboom F and MacManus-Driscoll J L 2015 Research update: atmospheric pressure spatial atomic layer deposition of ZnO thin films: reactors, doping, and devices *APL Mater.* **3** 040701